Title

Characterization and preclinical evaluation of the cGMP grade DNA based vaccine, AV-1959D to enter the first-in-human clinical trials.

Authors

Petrushina, Irina
Hovakimyan, Armine
Harahap-Carrillo, Indira S
et al.

Publication Date

2020-06-01

DOI

10.1016/j.nbd.2020.104823

Peer reviewed

HHS Public Access

Author manuscript

Neurobiol Dis. Author manuscript; available in PMC 2022 January 20.

Published in final edited form as:

Neurobiol Dis. 2020 June ; 139: 104823. doi:10.1016/j.nbd.2020.104823.

Characterization and preclinical evaluation of the cGMP grade DNA based vaccine, AV-1959D to enter the first-in-human clinical trials

Irina Petrushina[a,1], **Armine Hovakimyan**[b,1], **Indira S. Harahap-Carrillo**[c], **Hayk Davtyan**[a,b,d], **Tatevik Antonyan**[b], **Gor Chailyan**[b], **Konstantin Kazarian**[b], **Maxim Antonenko**[b], **Amandine Jullienne**[a], **Mary M. Hamer**[e], **Andre Obenaus**[e,f], **Olga King**[b], **Karen Zagorski**[b], **Mathew Blurton-Jones**[a,d,g], **David H. Cribbs**[a], **Harry Lander**[b], **Anahit Ghochikyan**[b,*], **Michael G. Agadjanyan**[b,*]

[a]Institute for Memory Impairments and Neurological Disorders, University of California, Irvine, CA, USA

[b]Department of Molecular Immunology, Institute for Molecular Medicine, Huntington Beach, CA, USA

[c]Department of Basic Sciences, Loma Linda University School of Medicine, Loma Linda, CA, USA

[d]Sue and Bill Gross Stem Cell Research Center, University of California, Irvine, CA, USA

[e]Department of Pediatrics, University of California, Irvine, CA, USA

[f]Preclinical and Translational Imaging Center, University of California, Irvine, CA, USA

[g]Department of Neurobiology and Behavior, University of California, Irvine, CA, USA

Abstract

The DNA vaccine, AV-1959D, targeting N-terminal epitope of Aβ peptide, has been proven immunogenic in mice, rabbits, and non-human primates, while its therapeutic efficacy has been shown in mouse models of Alzheimer's disease (AD). Here we report for the first time on IND-enabling biodistribution and safety/toxicology studies of cGMP-grade AV-1959D vaccine in the Tg2576 mouse model of AD. We also tested acute neuropathology safety profiles of AV-1959D in another AD disease model, Tg-SwDI mice with established vascular and parenchymal Aβ pathology in a pre-clinical translational study. Biodistribution studies two days after the injection demonstrated high copy numbers of AV-1959D plasmid after single immunization of Tg2576 mice at the injection sites but not in the tissues of distant organs. Plasmids persisted at the injection sites of some mice 60 days after vaccination. In Tg2576 mice with established amyloid pathology, we did not observe short- or long-term toxicities after multiple immunizations with

[*]Corresponding authors at: The Institute for Molecular Medicine, 16371 Gothard Str., H, Huntington Beach, CA 92647, USA. aghochykyan@immed.org (A. Ghochikyan), magadjanyan@immed.org (M.G. Agadjanyan).

[1]These authors contributed equally to this study

Declaration of Competing Interest

Dr. Ghochikyan and Dr. Agadjanyan are co-authors of US patent 10005825 B2. Other authors declare no competing financial interests.

three doses of AV-1959D. Assessment of the repeated dose acute safety of AV-1959D in cerebral amyloid angiopathy (CAA) prone Tg-SwDI mice did not reveal any immunotherapy-induced vasogenic edema detected by magnetic resonance imaging (MRI) or increased microhemorrhages. Multiple immunizations of Tg-SwDI mice with AV-1959D did not induce T and B cell infiltration, glial activation, vascular deposition of Aβ, or neuronal degeneration (necrosis and apoptosis) greater than that in the control group determined by immunohistochemistry of brain tissues. Taken together, the safety data from two different mouse models of AD substantiate a favorable safety profile of the cGMP grade AV-1959D vaccine supporting its progression to first-in-human clinical trials.

Keywords

Alzheimer's disease (AD); DNA Aβ-vaccine; Biodistribution; Safety toxicology; Magnetic resonance imaging (MRI); Immunohistochemistry (IHC); Mouse models of AD

1. Introduction

The neuropathology of Alzheimer's disease (AD) includes deposition of Aβ fragments of amyloid precursor protein (APP) in senile plaques and blood vessels, accumulation of neurofibrillary tangles (NFT) composed of tau protein, synaptic dysfunction, and death of neurons. For over twenty years, Aβ peptides have been thought to play a central role in the onset and progression of AD (Selkoe, 1991; Selkoe, 1994), and the 'amyloid cascade hypothesis' has emerged from this proposal (Golde et al., 2006; Hardy, 2006; Hardy and Higgins, 1992). This hypothesis is focused on soluble oligomers and protofibrils of Aβ, which are now considered to be the most toxic forms of Aβ, responsible for synaptic destruction (Cleary et al., 2005; Cline et al., 2018; Haass and Selkoe, 2007; Klein et al., 2004; Lacor et al., 2007; Lambert et al., 1998; Shankar et al., 2007; Shankar et al., 2008; Smith and Strittmatter, 2017). The efficacies of Aβ-immunotherapeutics have been tested in various animal models of AD, resulting in promising data. The first vaccine clinical trial in AD patients (AN-1792) was unsuccessful due to a small but statistically significant incidence of meningoencephalitis, which was thought to be associated with autoreactive T cell infiltration into the brains of immunized subjects (Ferrer et al., 2004; Nicoll et al., 2003; Orgogozo et al., 2003). Another major issue with the AN-1792 vaccine was immunogenicity: a fraction of vaccinated subjects generated anti-Aβ antibody titers ≥2200, and only a small subset of vaccinated subjects induced therapeutically potent titers ≥10,000 of these antibodies. This was unfortunate because many clinical trials with passive vaccines suggested that the therapeutic effect of anti-Aβ antibodies was dose-dependent (Bachmann, 2019; Boche et al., 2008; Gilman et al., 2005; Holmes et al., 2008; Nicoll et al., 2003; Selkoe, 2018; Sevigny et al., 2016).

To avoid autoreactive T cells against Aβ and generate relatively high concentrations of antibodies, it was proposed by various groups, including ours, to develop vaccines by removing T-cell epitopes of $A\beta_{42}$, which were responsible for initiation of meningoencephalitis, and using B-cell epitopes of a self-peptide fused with a carrier capable of stimulating harmless T-cell responses against foreign carrier-molecules (Agadjanyan et

al., 2005; Arai et al., 2015; Davtyan et al., 2014a; Lemere and Masliah, 2010; Lobello et al., 2012; Marciani, 2016; Petrushina et al., 2007; Ryan and Grundman, 2009; Schneeberger et al., 2010; Wang et al., 2007; Wang et al., 2017; Winblad et al., 2012; Winblad et al., 2009). Unfortunately, to date only limited clinical data have been published on such epitope vaccines which prevents estimation of the immunogenicity of such vaccines against Aβ (Arai et al., 2015; Marciani, 2016; Schneeberger et al., 2010; Wang et al., 2017; Winblad et al., 2012). This is regrettable, because the dose-dependent effectiveness of passively administered anti-Aβ antibodies specific to oligomers/protofibrils, was recently demonstrated in subjects with mild AD (Bachmann, 2019; Neurimmune, 2015; Selkoe, 2018; Sevigny et al., 2016). Although phase 3 trial of aducanumab was recently halted due to of lack of efficacy in the interim analysis (Selkoe, 2019), an expanded dataset from the phase 3 EMERGE trial on patients receiving high-dose aducanumab reported statistically significant changes in the Clinical Dementia Rating-Sum of Boxes (CDR-SB) scores (Haeberlein et al., 2019). These data are very encouraging for AD patients. They indicate that, firstly, a treatment should be started in asymptomatic at-risk individuals before irreversible neurodegeneration has occurred, and secondly, high antibody titers are required to achieve effectiveness. Thus, an Aβ vaccine needs to be administered preventatively to halt or at least delay the development of AD pathology.

Over the past 18 years, we have developed first, second, and third-generation epitope vaccines, comprising the N-terminus of Aβ and various foreign T helper (Th) epitopes. The immunogenicity of one such third-generation DNA-based vaccine, AV-1959D encoding protein composed of three copies of Aβ B cell epitope ($Aβ_{1–11}$) fused to MultiTEP platform, a string of 12 non-self, pathogen-derived Th epitopes, was previously tested in mice, rabbits and non-human primates (Davtyan et al., 2014a; Davtyan et al., 2014b; Evans et al., 2014; Ghochikyan et al., 2013). Delivered by electroporation (EP), the AV-1959D vaccine generated a robust cellular immune response to foreign epitopes, avoided activation of potentially harmful autoreactive T cells, and induced strong and therapeutically potent anti-Aβ antibodies in all animal species tested (Davtyan et al., 2014a; Davtyan et al., 2014b; Evans et al., 2014; Ghochikyan et al., 2013). Interestingly, in nonhuman primates (NHP), the AV-1959D vaccine activated a broad repertoire of T helper cells, indicating that such a vaccine might overcome MHC class II polymorphism. The AV-1959D vaccine may also activate both naive and memory Th cells, which could be beneficial in overcoming the age-associated changes in T-cell immunity resulting in decreasing proportions of naive cells and increasing proportions of memory cells in humans (Derhovanessian et al., 2008). Considering that the Th epitopes were selected based on their ability to bind various human MHC class II molecules, we expect that all vaccinated subjects would respond to the vaccine by activating T cells specific to at least one Th epitope incorporated in MultiTEP vaccine platform and thereby producing high titers of anti-Aβ antibodies. Importantly, epitope vaccines targeting the $Aβ_{1–11}$ peptide reduced amyloid pathology and improved behavior in mouse models of AD (Davtyan et al., 2013; Movsesyan et al., 2008a; Petrushina et al., 2017). Based on these published results, we conducted biodistribution/persistence, acute and long-term safety/toxicology studies of cGMP grade AV-1959D DNA vaccine delivered by electroporation.

Here we present the data generated in two separate studies. In the first study, we analyzed safety/toxicity/biodistribution of AV-1959D DNA vaccine in well-established Tg2576 mouse model of AD. In the second study, we used Tg-SwDI mice as an early-onset CAA model (Davis et al., 2004; Klohs et al., 2014; Miao et al., 2005a; Miao et al., 2005b) that was more appropriate for analyzing whether AV-1959D vaccine can worsen CAA, induce vasogenic edema or hemorrhages, and increase inflammation.

2. Materials and methods

Mice.

Biodistribution/persistence, acute and long-term safety/toxicology studies were performed in Tg2576 mice. For a comprehensive evaluation of the AV-1959D safety profile, we analyzed neuropathological changes in Tg-SwDI mice, which show early-onset cerebral microvascular amyloidosis in the form of fibrillar vascular Aβ deposits starting at the age of 6 months (Davis et al., 2004; Davis et al., 2006; Vasilevko et al., 2007; Yang et al., 2011). Female and male Tg2576 (H-$2^{b/s}$ haplotype) and Tg-SwDI (H-2^{b} haplotype) mice purchased from JAX ® Lab were bred at the animal care facility of the University of California, Irvine. All animals were housed in a temperature and light-cycle controlled facility, and their care was under the guidelines of the National Institutes of Health and an approved IACUC protocol at the University of California, Irvine.

2.1. Design of DNA vaccine

AV-1959D vaccine encoding protein composed of three copies of $A\beta_{1–11}$ (e.g., B cell epitope of amyloid) linked to MultiTEP platform (e.g., string of twelve foreign Th epitopes) was generated as previously described in (Evans et al., 2014; Ghochikyan et al., 2013). Briefly, *3Aβ$_{1–11}$-PADRE* minigene fused to mouse Igκ-chain signal sequence was synthesized as previously reported (Movsesyan et al., 2008a; Movsesyan et al., 2008b) using overlapping PCR technique. A polynucleotide encoding multiple T helper epitopes (MultiTEP platform) from Tetanus Toxin (TT) (P2 P21, P23, P30, P32, P7, P17, and P28), hepatitis B virus (HBsAg, HBVnc) and influenza (MT) separated by GS linkers was synthesized by GenScript and fused with *3Aβ$_{1–11}$-PADRE* minigene by overlapping PCR. The resulting gene was cloned into the pVAX1 vector designed to be coherent with current Food and Drug Administration (FDA) guidelines (1996), using *NheI*/BamH1 restriction sites. DNA sequencing was performed to confirm that the generated plasmids contained the correct sequences. The resultant plasmid was designated as AV-1959D.

2.2. Preparation of Master cell bank (MCB) and manufacturing of AV-1959D

The MCB preparation and the AV-1959D vaccine (e.g., drug substance) manufacturing were conducted under current good manufacturing practice (cGMP) at Ajinomoto Althea, Inc. (San Diego, CA). Briefly, *E. coli* K-12 DH10B strain was transformed with AV-1959D plasmid and kanamycin positive clones were selected. Plasmid DNA was purified from five single colonies and analyzed by electrophoresis. Based on these results, clones yielding higher covalently closed circular, higher quality (low RNA, low “nicked” plasmid and low dimer) plasmid DNA were identified and used for cell banking. For cell banking, the flask containing 400 ml LB/kanamycin was inoculated with 800 μl culture of the chosen clone

and incubated in incubator-shaker at 37 °C 220–275 rpm. When OD_{600} reached 1.9491, incubation was stopped. 60 ml of 80% sterile glycerol stock solution was added to 260 ml culture for a final glycerol concentration 15%. This MCB designated as pIMS488 and 1 ml ± 0.1 ml was aseptically aliquoted into cryovials. Each cryovial was inspected visually, labeled, and stored at −80 °C.

To manufacture AV-1959D, a vial of pIMS488 MCB was thawed and used for fermentation under the strictly controlled growth parameters. After fermentation, the cells were harvested by UF/DF and lysed. The crude plasmid DNA is further purified by a single chromatography step with multiple washes, and an additional chromatography polishing step. The resulting plasmid DNA was precipitated with IPA, centrifuged, and dried, then was resuspended in PBS buffer, filtered through a 0.2 μm membrane and stored in a cold storage unit until transfer to Fill/Finish for the drug product filling. The concentration of the final plasmid was 3.7 mg/ml, and this AV-1959D was used for all preclinical studies described below.

2.3. Immunization of mice and analyses of humoral immune responses

The animals were anesthetized using 2% isoflurane during the dosing procedures. Mice were injected in right flank near the base of the tail with a dose of AV-1959D in 30 μl PBS. Immediately after DNA administration, a needle electrode made of two parallel rows of six 2-mm needles 0.3 mm in diameter (1.5 × 4-mm gaps) was inserted into the skin around the swollen area of injection, and pulses were applied using the AgilePulse™ device. The 30-gauge Insulin Syringes with the BD Ultra-Fine needle (BD, Franklin Lakes, NJ) were used for i.d. injections. Control mice were injected with PBS followed by electrical pulses.

Anti-Aβ antibodies were detected in sera of vaccinated mice using ELISA, as described previously (Davtyan et al., 2010; Ghochikyan et al., 2006; Petrushina et al., 2007). In safety/toxicology studies, blood of vaccinated Tg2576 mice was collected for analysis for anti-Aβ antibodies at days 1 (before immunizations), 56 (after three immunizations), 86 (after four immunizations) and at termination time points at 76, 102 and 158 days. In the neuropathological safety study, blood of vaccinated Tg-SwDI mice was collected on days 2 and 14 after the last immunization. All the samples were analyzed in duplicate, and mean values of the concentrations were used in the analyses. Briefly, wells of 96-well plates (Immulon II; Dynatech Laboratories, VA) were coated with 2.5 μM soluble $A\beta_{42}$ (pH 9.7, o/n, and 4 °C). The wells were washed and blocked with 3% non-fat dry milk in Tween-20 Tris Buffer Solution (TTBS) and serial dilutions of primary sera were added to the wells and incubated overnight at 4 °C. After incubation and washing HRP-conjugated anti-mouse IgG was added as recommended by the manufacturer (Jackson Labs, ME). Plates were incubated for 2 h at room temperature, washed, and the reaction was developed by adding *3,3′,5,5′tetramethylbenzidine* (TMB) substrate solution, and stopped with 2 N H_2SO_4. The optical density (OD) was read at 450 nm (Biotek, Synergy HT, VT), and antibody concentrations were calculated using a calibration curve generated with 6E10 monoclonal antibody (Biolegend, San Diego, CA).

2.4. Biodistribution/persistence studies

4–5 mo old Tg2576 male and female mice (n = 52) were assigned to either vaccine (n = 16F/16M) or control (10F/10M) groups (Table 1). All animals in the vaccine group were immunized with 50 μg of AV-1959D, and control mice were injected with PBS followed by electroporation-mediated intradermal injection as described above. At termination (days 2 or 60) blood was collected and mice were then humanely euthanized. Selected tissues (blood, bone marrow (femur), brain, heart, injection site, lungs, inguinal lymph nodes, ovaries, kidneys spleen, liver, testes) were collected for qPCR (quantitative polymerase chain reaction) analysis. Additional tissues (adrenals, pancreas, skeletal muscle, spinal cord, stomach, thymus, mesenteric and submaxillary lymph nodes) were collected and held for future analysis if requested by FDA.

DNA from selected tissues was isolated using the Qiagen DNeasy kit. qPCR assay was performed with primers/probe designed to detect 76 bp sequence present on AV-1959D plasmid in the region encoding MultiTEP. The forward primer anneals to the sequence encoding P32 Thepitope (5′CACCAAACAACGAGATCGACTCT3′), reverse primer (5′TGCACCGATCCAGCTTCAG 3′) and probe (5′ AAGCATCCGGGAGGACAACAACATCA 3′) anneals to the sequence encoding P21 Th epitope of MultiTEP. The qPCR assay was first validated (sensitivity, accuracy, precision, specificity, limit of detection (LOD), limit of quantification (LOQ), Linearity) using organ tissues from naïve mice with spiked plasmid. All assay validity criteria met the following recommendations:

2.4.1. Accuracy/Sensitivity—For the 50 copies positive control DNA standard post-spiked into 1 μg of DNA isolated from each naïve tissue, the mean determined copy number must be ≥ 25 copies.

2.4.2. Precision (Intra-Assay Repeatability)—The % RSD of the 9 replicates of the 50 copies of positive control DNA standard within one run must be ≤ 30%. The % RSD of the three replicates of the post-spiked samples within the assay must be ≤ 60%.

2.4.3. Specificity—One μg of DNA isolated from each naïve tissue must have a PCR amplification signal corresponding to < LOQ.

2.4.4. Limit of Quantitation (LOQ)—The LOQ of the assay must be ≤10 copies of positive control DNA standard in the presence of 1 μg mouse DNA.

2.4.5. Linearity and slope—All assays require an R^2 value of ≥0.95 and a slope value of −3.0 to −4.0. The range over which the assay has an R^2 value of ≥0.95 and a slope value of −3.0 to −4.0, must include 1×10^1 copies to 1×10^5 copies of positive control DNA standard in the presence of 1 μg mouse DNA. DNA isolation and detection of plasmid DNA in the tissues from various organs of control and vaccinated mice was performed by WuXi AppTec, Philadelphia. WuXi AppTec determined the limit of detection (LOD) as 1 copy/μg of genomic DNA, the limit of quantification (LOQ) as 10 copies/μg of genomic DNA. Positive was defined as ≥100 copies/μg of genomic DNA.

2.5. Acute and long-term safety/toxicology studies

Tg2576 male and female mice aged (9–10 months) (n = 144F/144M), were transferred to WuXi AppTec. Upon arrival, animals were quarantined for 30 days (± 7 days). One week prior to dosing, animals were weighed and systematically assigned to 12 subgroups, divided among 4 treatment groups, based on body weights. There were three subgroups per each treatment group that corresponded to a sacrificial end-point (Table 2). Mice received four (at days 0, 14, 44, 74) EP-mediated intradermal injections with 5 μg (low), 25 μg (optimal), or 50 μg (high) of AV-1959D. The "optimal" dose was the dose that induced the highest immune response, where lower doses induced a lower response and higher doses did not improve or even decreased vaccine efficacy. In this case, injection of mice with 25 μg DNA resulted in the highest immune response with low variability and high reproducibility. Blood samples were collected at indicated time points and at scheduled terminal time points from animals in each group. A full panel of tissues (42) was prepared for histopathology from mice taken at the scheduled terminations.

2.6. Acute neuropathology studies

10–11 mo old male and female Tg-SwDI mice were vaccinated with high dose (50 μg/mouse) of AV-1959D at days 0, 14, 44, 74. Titers of antibodies were measured at termination on days 76 (2 days after the last immunization) and 88 (14 days after the last immunization). Animals were randomly allocated for the neuropathology assessment via IHC and histochemistry (main cohort, n = 7 or 8, 2d/14d time-points, males/female, control/immunization; total n = 59 animals). A separate MRI study was conducted for day 2 and 14 assessments (n = 8, males/female, control/immunization; total n = 32 animals) in vaccinated and control groups.

2.7. Brain collection

Prior to the brain collection, mice were anesthetized with an intraperitoneal injection of 150 mg/kg Nembutal Sodium Solution (Akorn, Inc., Lake Forest, IL), then perfused with 36 mL of 1xPBS (pH 7.4) using a peristaltic pump (12 mL/min). Brains were extracted and postfixed in 4% PFA for 24 h, washed in PBS, and immersed in 20% sucrose overnight and sectioned at 40 μm thickness using the microtome (Leica SN2010R). Sections were collected into 12-well plates to obtain the series of equally-spaced sections throughout each brain.

2.8. Immunohistochemistry and histochemistry

The vascular deposition of Aβ, glial activation, astrocytosis, T and B cell infiltration as well as neuronal degeneration were analyzed in brain sections of vaccinated and control mice sacrificed at days 2 and 14 after the last immunization. The levels of microgliosis were identified using Iba1 Rabbit polyclonal antibody (GTX100042, GeneTex) at 1:500 dilution utilizing 0.1 M citrate buffer pretreatment; for detection of mouse astrocytes we used Rabbit polyclonal Glial Fibrillary Acidic Protein (GFAP, RB-087-A, Thermo Fisher Scientific) at 1:500; for analyzing possible T cell infiltration, we utilized Rabbit monoclonal [SP7] antibody to CD3 (ab16669, Abcam) at 1:500; for detection of B-cells, we used Rabbit recombinant monoclonal purified Ab B220 [BL-178–12C7] (A700–012, Bethyl

Laboratories) at 1:250, with a 0.1 M citrate buffer pretreatment. Histological staining for brain hemosiderin deposits to detect microhemorrhages was performed using the Iron Stain kit (#87006, Thermo Fisher Scientific) according to manufacturer's instructions. Counts of hemosiderin profiles for both were made semi-quantitatively by two independent researchers spanning the entire brain using whole-slide images at 10 × magnification of 13 equally-spaced brain sections. For cerebral amyloid angiopathy (CAA) detection, vascular Aβ deposits were visualized using Thioflavin S (ThS; Sigma-Aldrich), performed as described previously (Movsesyan et al., 2008a; Petrushina et al., 2007). Neurodegeneration was assessed via detection of cleaved caspase-3 binding using a rabbit mAb (Asp 175) (5A1E, #9664, Cell Signaling Technology) at 1:200; as well as utilizing TUNEL (terminal deoxynucleotidyl transferase dUTP nick end labeling) assay kit for apoptotic detection designed for neuronal tissue - Neuro-TACS II In Situ Apoptosis Detection kit (#4823–30-K, Trevigen) according to manufacturer's instructions.

2.9. Whole-slide imaging and data analysis

Three 40 μm brain section panels equally spaced at the same level between Bregma points − 0.22 and − 2.70 mm were analyzed for all staining experiments with two exceptions. Assessment of microhemorrhages utilized Prussian blue staining on thirteen sections per brain equally spaced between Bregma points 1.18 and − 4.24 mm, and in the TUNEL assay was performed on one section per brain at approximately −1.94 mm Bregma.

The whole slide imaging for all assays was provided by Alafi Neuroimaging laboratory at Washington University School of Medicine (St. Louis, MO). The slides were digitized using a whole slide scanner (Nanozoomer 2.0 HT, Hamamatsu, Bridgewater, NJ). Quantification using digital pathology software (Visiomorph, Broomfield, CO) was performed for Thioflavin S, Iba1, GFAP, and Cleaved Caspase-3 images. All other images underwent semi-quantitative analyses via visual inspection by two independent observers blinded to treatment conditions to determine mean semi-quantitative scores.

2.10. MRI imaging and data analysis

The brains of immunized mice and control animals were assessed for vasogenic edema (VE) and microhemorrhages using MRI on day 2 and 14 after the last immunization. Data obtained by MRI were compared to brain sections with histologically detected microhemorrhages. For MRI imaging, a cohort of 32 Tg-SwDI mice 10–11 mo old (n = 8 for each group including male, female, control and experimental groups) was treated according to vaccination protocol. All imaging was performed at Loma Linda University on an 11.7 T Bruker Avance MRI (Bruker Biospin, Billerica, MA). Animals were transported in 2 shipments within 24 h after immunization. Mice were imaged in vivo at 2 days post-treatment and were lightly anesthetized with isoflurane (3% induction, 1% maintenance) and placed in a volume receive only radiofrequency coil. Body temperature was maintained at 37 °C by using a water-heated pad. In vivo T2 weighted images for edema (T2WI, TR/TE = 3000 ms/10 ms, 25 × 0.5 mm slices, matrix 192 × 192) and susceptibility-weighted images for microhemorrhages (SWI; TR/TE = 617.7 ms/7 ms, 25 × 0.5 mm slices, matrix 256 × 256) were collected with a 2.2 cm field of view for a total imaging time of 25 min.

After imaging, mice were allowed to recover on a heated surface until ambulatory and then returned to their cage.

Due to a radiofrequency coil failure, we were unable to image in vivo at 14 days post-treatment as planned but performed ex vivo imaging. Mice at 14 days post-treatment underwent intracardial perfusion for brain fixation, as previously reported (Obenaus et al., 2017). Briefly, mice were anesthetized with an intraperitoneal injection of ketamine (90 mg/kg) and xylazine (10 mg/kg), then perfused with 10 mL of 1XPBS (pH 7.4) and 30 mL 4% PFA (pH 7.4) using a peristaltic pump (8.4 mL/min). Brains were extracted and postfixed in 4% PFA for 24 h. Brains were then rinsed and stored in PBS at 4 °C until imaging. Brains were imaged ex vivo using the same parameters as noted above, except with a 1.7 cm field of view.

T2WI data were processed for T2 maps, which report tissue relaxation properties (ms) and can report the presence of edema similar to previously published methods (Ghosh et al., 2012). Multiple regions of interest (ROIs) were manually drawn on T2WI using Cheshire (Parexel International Corp. Waltham, MA, USA), and the ROIs were then transferred to T2 maps to extract average T2 values (ms) from each ROI. Bilateral brain ROIs included cortex and striatum at the level of the dorsal hippocampus. T2 images were also used to calculate whole brain (WB) and ventricular volumes.

SWI was used to quantify micro-hemorrhages that appear as hypo-intensities. All SWI data were processed using SPIN (MRI Institute, Detroit, MI, USA) as previously described (Baghchechi, 2016). Using minimum intensity projection images (MIPs), focal hypo-intensities were manually quantified by an experimenter blinded to the animal groups for the cortex, striatum, and brainstem regions at days 2 and 14 post-immunization.

2.11. Statistical analysis

Statistical parameters (mean, standard deviation (SD), significant differences, etc.) were calculated using the Prism 6 software (GraphPad Software, Inc., La Jolla, CA). Statistically significant differences were examined using a two-tailed *t*-test and 2-way ANOVA, Tukey's multiple comparison tests (a P value of less than 0.05 was considered significant).

3. Results

3.1. Biodistribution/persistence of AV-1959D plasmid in Tg2576 mouse model of AD

In GLP biodistribution/persistence studies, Tg2576 mice received a single EP-mediated injection with a high dose (50 μg/mouse) of AV-1959D (Table 1). Mice were terminated on day 2 or 60 after the immunization, blood, and 19 selected tissues were collected for qPCR and archived.

The first phase of biodistribution analysis of samples collected on day 2 involved a subset of eleven tissues (blood, heart, lung, liver, spleen, kidney, brain, bone marrow, testis/ovaries, the inguinal lymph nodes and skin from an injection site), while other tissues were archived for possible future analyses based on the results of this initial study.

Biodistribution analyses were conducted following the FDA recommendations specifying "that the sensitivity of this assay be sufficient to quantify < 100 copies of plasmid per microgram of host DNA. A claim of 'non-persistence' requires that the amount of plasmid at each site falls below this limit of quantification" (FDA, 2007). As expected, by qPCR we detected high numbers of plasmid copies (ranging from 3794 to 185,292,500 copies) at the injection site (skin), which is the sine qua non of generation of good immune responses (Fig. 1). We observed high variability in plasmid copy numbers at the injection site, which may be associated with skin tissue susceptibility to electrical pulses in individual mice. Some inter-individual variability was also observed in tissues from male mice compared to females; however, these sex-related differences were non-significant. Copy numbers in the tissues from distant organs in female and male mice did not exceed 100 copies/μg of genomic DNA except in bone marrow from one male mouse and inguinal lymph nodes from another male mouse in which the copy numbers were slightly higher than 100. All tissues were harvested (and archived) from day 60 animals and plasmid persistence was evaluated in tissues from distant organs where plasmid copy number > 100 copies/μg of genomic DNA was found at day 2, in bone marrow and lymph node tissues from male mice only, as well as in skin tissues (injection site) collected from all mice. The most important issue associated with DNA vaccines is the possible integration of the plasmid into the chromosome. Typically integration studies are warranted only when plasmid persists in any tissue of any animal at levels exceeding 30,000 copies per μg of host DNA by study termination. On the 60th day after the injection, we detected 5626, 5319, 4529, and 151 copies of plasmid per 1 μg genomic DNA in the injection sites of two male and two female mice, respectively. Therefore, we did not analyze the plasmid persistence at later time points. Day 2 results demonstrated that no control PBS-injected mice were found to be positive for AV-1959D DNA (data not shown).

3.2. Safety and tolerability of AV-1959D in Tg2576 mouse model of AD

GLP studies on acute and long-term safety/toxicology of the vaccine were performed in aged Tg2576 mice possessing β-amyloid pathology (both intracellular Aβ and plaques) after EP-mediated intradermal administration of repeat doses of AV-1959D or PBS (Table 2). Although we previously showed that antibodies targeting the N-terminus of Aβ could reduce pathology only in the preventive, but not therapeutic vaccination of Tg2576 mice (Petrushina et al., 2017), safety/toxicology studies were conducted in aged Tg 2576 mice to explore the vaccine effects in animals with existing Aβ plaque deposits in the brain and cognitive deficits.

As shown in Table 2, Tg2576 mice were immunized with three different doses of AV-1959D, followed by EP. Dose consideration was based on the optimal immunogenic dose of AV-1959D in mice (25 μg/mouse). In the safety/toxicology studies, the FDA required testing doses that are lower and higher than the optimal dose where the high dose should be at least ten-fold higher than that expected for future clinical trials (calculated as dose/kg). These doses, calculated per kg (~200 μg/kg, ~1000 μg/kg and ~2000 μg/kg), are about 14, 70 and 140 fold higher than the maximal dose expected for use in humans (1000 μg/subject or ~14 μg/kg for human with average weight 70 kg).

We verified humoral immune responses in immunized mice and demonstrated that vaccinations induced anti-Aβ antibodies in all mice (Fig. 2). In general, 25 μg/mouse (optimal) and 50 μg/mouse (high) doses of vaccine generated similar levels of humoral immune responses, while the low dose induced a lesser amount of anti-Aβ antibodies. In female animals immunized with low dose, we observed significantly higher humoral immune response to the vaccine than in males on days 76 and 158. A low response in males on day 76 (32 days after the third immunization and two days after the 4th immunization) and day 158 (84 days after the last immunization) indicates that antibody levels in male mice decline faster than in female mice. Antibody levels declined faster in mice immunized with 5 μg/mouse dose compared to mice immunized with 25 μg/mouse and 50 μg/mouse on day 158, three months after the last immunization.

Under the conditions of this study, there were no adverse findings in health observations, food intake, body weights, gross necropsy, absolute organ weights or weight ratios, clinical pathology (hematology/coagulation parameters, clinical chemistry) nor in histopathology data attributed to the AV-1959D vaccine. Except for the minimal reactions at the injection site, the findings were consistent with the Tg2576 mouse model (parenchymal plaques and vascular amyloid deposits), normal aging, or background lesions/changes found in laboratory rodents. The results suggest that AV-1959D dosed at levels of 5, 25 and 50 μg does not result in acute or long-term immunotoxicity in Tg2576 mice, especially when administered to males and females via four-repeated EP-mediated intradermal injections (days 1, 14, 44 and 74) with a study duration of 158 ± 2 days.

3.3. Neuropathological analysis of Tg-SwDI mice vaccinated with AV-1959D

In the light of the adverse events reported for AN-1792 active vaccination, the FDA recommended conducting an extensive neuropathology evaluation (meningeal-related inflammation, microhemorrhage, vascular degeneration, vasogenic edema, & necrosis, etc.) on brain sections of APP/Tg mice that possess anti-Aβ-antibody responses. Therefore, 10-11mo old Tg-SwDI mice, which show early-onset cerebral microvascular amyloidosis (Davis et al., 2004; Davis et al., 2006; Vasilevko et al., 2007; Yang et al., 2011), were administered with 50 μg/mouse (high dose) AV-1959D via four-repeated EP-mediated intradermal injections at time points days 1, 14, 44 and 74. To confirm that AV-1959D induced humoral immune responses, we measured anti-Aβ antibodies on day 76 and day 88 (2 and 14 days after the last immunizations) in male and female mice. As shown in Fig. 3, all mice responded to the vaccine by generation of anti-Aβ antibodies, and the response was higher at day 14, at the expected *peak* of the *immune response*. Next, we evaluated the acute safety of AV-1959D by analyzing all neuropathological changes in brains of Tg-SwDI mice by MRI, IHC, and histochemistry.

3.3.1. MRI quantitative analysis found no signs of vasogenic edema or microhemorrhages in Tg-SwDI mice vaccinated with AV-1959D—

Non-invasive MRI was performed using quantitative T2-weighted imaging (T2WI) for edema (water content) determination. Susceptibility weighted imaging (SWI) was utilized for the assessment of microhemorrhages, as evidenced by iron-induced dephasing (SWI hypo-

intensities). All MRI investigations were performed at 2 and 14 days after the last vaccination in male and female Tg-SwDI mice.

There were no overt differences observable on any of the T2WI nor the quantitative T2 maps (Fig. 4A). The lack of visible hyperintense signals on T2WI in either male/female or control/immunized groups lead us to examine quantitatively if there were increases in water content in the cortex or striatum. In the cortex, when right and left regions were combined, there were no significant increases in water content at day 2 post-immunization (Fig. 4B) between males/females and their respective control or immunized treatments. At day 14 post-immunization, there were also no significant increases in edema (T2 values) in the cortex (Fig. 4C). We also assessed the striatum in these rodents, and no significant increases in T2 (edema) were found between male/female or control/immunized animals (data not shown). Thus, anti-Aβ immunotherapy does not significantly modify water content in the cortex or striatum at 2 or 14 days after the last immunization.

Whole-brain (WB) volumes were assessed from T2WI MRI where we observed that male brains were significantly smaller than female brains ($p < .05$) (Fig. 4D), but within control and immunized male or female cohorts no significant differences in brain volume were observed. Given the increased brain size in female brains, we measured ventricular volumes from MRI but found no significant differences between any of the groups (Fig. 4E) (two-way ANOVA, Tukey's multiple comparisons, NS $p > .05$). Thus, our data suggest that anti-Aβ immunotherapy does not significantly modify water content, brain size, or ventricular volumes in the brain of PBS injected or AV-1959D vaccinated mice at 2 or 14 days after treatment.

MRI derived magnitude and phase images were processed to enhance the visualization of hypo-intensities on SWI (Baghchechi, 2016). Micro-hemorrhage hypo-intensities were readily observed on maximum intensity projection images and then counted within cortical, striatal and brainstem regions spanning the entire brain (Fig. 5). Similarly, at day 2 post-immunization, there were no significant differences between groups across the anterior-posterior extent of the brain (Fig. 5B), nor when the numbers of hypo-intensities across all brain slices (8–10 mm) were quantified (Fig. 5C).

We performed similar empirical studies at day 14 post-immunization (Fig. 5D, E) that were acquired ex vivo, which is known to improve data quality (Fig. 5A). While anterior-posterior assessment of hypo-intensities at day 14 were not significantly different between controls or immunized groups (Fig. 5D), we did observe increased numbers of hypo-intensities at the level of the dorsal hippocampus (see Fig. 5A) primarily within the striatum (see also Fig. 6A). The increase in the anterior-posterior extent was significantly different in males (two-way ANOVA, Tukey's multiple comparisons; $p < .0001$) with no anterior-posterior variations in females (Fig. 5D). However, when all the hypointensities throughout the brain were averaged together, no significant differences were observed between groups or within genders (Fig. 5E). Thus, similar to the day 2 data, no significant differences in microhemorrhages were observed at day 14 post-immunization by MRI. The apparent increase in the number of microhemorrhages at the level of the dorsal hippocampus in males (irrespective of control or immunization) requires further investigation.

3.3.2. Histological verification of the MRI data on lack of AV-1959D-induced microhemorrhages in Tg-SwDI—Corresponding sections of the brains of Tg-SwDI vaccinated and control mice used in MRI were stained with Prussian Blue to confirm the presence of microhemorrhages (see Fig. 5). More specifically, we undertook histological verification of SWI MRI data at day 14, and the presence of iron and iron products was evaluated (Fig. 6). In male and female Tg-SwDI mice, there were observable overt hypointensities in both genders, but that was more prominent in males (Fig. 6A). Histology affords greater precision at the micrometer scale compared to the millimeter scale of MRI, as can be observed with increasing magnification. Indeed, large Prussian blue aggregates are present in histology that correspond to virtually similar regions of hypointensity on SWI MRI (despite the large pixel size on MRI). Quantification confirmed that the total number of iron puncta and aggregates were similar between males and females, with no significant differences between the vaccinated and control groups (Fig. 6B). Similar to SWI findings (Fig. 5E), certain slices in males tended to have larger aggregates and numbers of iron staining compared to females, but no significant differences were observed (Fig. 6B). Thus, histological quantification confirmed that immunization does not appear to overtly alter the appearance of microhemorrhages in either male or female cohorts.

Separate groups of experimental and control Tg-SwDI mice ($n = 59$) that were not used in MRI studies were also used in histochemical analyses. Prussian blue staining of whole mouse brains confirmed no shifts in numbers of microhemorrhages in the brains of Tg-SwDI mice vaccinated with AV-1959D compared to control mice either on day 2 or day 14 after the last immunization (Fig. 7A,B). Therefore, these independent studies in separate groups of experimental and control Tg-SwDI mice confirmed the results in the MRI cohort (Figs. 5 and 6) and supports that AV-1959D does not enhance microhemorrhages in vaccinated animals.

3.3.3. AV-1959D does not increase Aβ vascular deposition in Tg-SwDI vaccinated mice—Next, we analyzed the effects of vaccination on cerebral amyloid angiopathy (CAA). The number of blood vessels showing amyloid depositions were determined in ThS-stained brain sections where vaccination with AV-1959D did not increase deposition of Aβ in blood vessels evaluated on day 2 or 14 after the last immunization (Fig. 8A,B) compared to control mice. No differences were observed between male and female mice.

3.3.4. Vaccination with AV-1959D does not increase inflammation in aged Tg-SwDI mice—To assess the scope of inflammation-related pathology in the brains of animals immunized with the AV-1959D, we examined glial activation. Staining with ThS did not reveal dense core plaques in these 14 mo old Tg-SwDI mice. In the absence of dense-core amyloid plaques, microglia are strongly associated with the amyloid-laden microvessels (Miao et al., 2005b) and Iba-1 positive microglia follow patterns of amyloid angiopathy closely in this model (Davis et al., 2004; Kruyer et al., 2015). The effect of vaccine on Iba1 positive microglia was quantitatively throughout the entire brain but no significant differences in the patterns of microglial activation in Tg-SwDI male and female

mice vaccinated with AV-1959D compared to control mice was found (days 2 or 14 post last immunization) (Fig. 9).

Next, we evaluated the extent of astrocytic cell activation in the brains of vaccinated and control mice using GFAP, a prototypical marker for immunochemical identification of astrocytes. It is regarded as a sensitive and reliable marker that labels most, if not all, reactive astrocytes in Tg-SwDI mice (Miao et al., 2005b; Passos et al., 2013). Quantitative image analysis of GFAP labeling throughout the whole brain showed no significant differences in the patterns of astrocyte activation in Tg-SwDI male and female mice vaccinated with AV-1959D compared to control mice either on day 2 or 14 post last immunization (Fig. 10).

We also investigated whether immunization with the AV-1959D might induce lymphocyte infiltration into the brains of Tg-SwDI mice. Brain sections of immunized and control mice were stained with anti-CD3 and anti-B220 antibodies for detection of T and B cells, respectively. As shown in Fig. 11, only a few cells were detected throughout the brains of vaccinated and control mice. Therefore, vaccination of Tg-SwDI mice with AV-1959D does not affect BBB and lymphocyte infiltration of the brain. Moreover, we saw significantly lower numbers of $CD3^+$ T cells in the brains of vaccinated compared with control mice terminated at day 14 after the last immunization ($p = .0093$). Therefore, IHC data suggest that no glial activation nor T and B cell brain infiltration were induced in the brains of Tg-SwDI mice vaccinated with AV-1959D.

3.3.5. Vaccination with AV-1959D did not induce neuronal degeneration in the brains of Tg-SwDI mice—To determine whether vaccination leads to neuronal degeneration, we assessed necrosis and apoptosis via terminal deoxynucleotidyl transferase dUTP nick end labeling (TUNEL) and cleaved caspase-3 activation. In TUNEL, DNA double-strand breaks and fragmentation were assessed in connection with the CAA pathology. The Tg-SwDI mouse model accumulates CAA primarily in the thalamic and hippocampal areas (Davis et al., 2004; Kruyer et al., 2015). The thalamus, dorsal hippocampus, and subiculum at the level of −1.94 mm Bregma were chosen for quantification. We were able to identify no significant differences and minimal pathological profiles in the cortex, caudate putamen, nerve fiber tracts, and hypothalamus regions, between the vaccinated and control mice. Anti-caspase-3 immunostaining revealed few pathological profiles throughout the whole brain, including thalamic, cortical, hippocampal, corpus callosum areas. No significant differences were observed in the number of TUNEL-positive (A) and cleaved caspase-3 positive (B) apoptotic cells between AV-1959D vaccinated and PBS-injected mice (Fig. 12). Therefore, AV-1959D vaccination did not induce neuronal degeneration in aged Tg-SwDI mice.

4. Discussion

Active vaccines generating antibodies specific to N-terminus of Aβ as well as passive administration of Mab with the same specificity reduce AD-like pathology in animal models of AD (Agadjanyan et al., 2015; Spencer and Masliah, 2014) and Aβ-pathology in the brains of AD patients (Ferrer et al., 2004; Kerchner and Boxer, 2010; Nicoll et al., 2006; Nicoll

et al., 2003). The goals of this study were (i) comprehensive assessment of biodistribution and safety/tolerability of AV-1959D vaccine, generating anti-$A\beta_{1–11}$ specific antibodies, in Tg2576 mice with established Aβ pathology and (ii) evaluation of acute neuropathology safety profiles of this vaccine in CAA prone Tg-SwDI mouse model of AD.

Immunotherapeutic strategies displayed great promise in animal models of AD and strong efforts were made by industry to inhibit the generation of toxic Aβ aggregates and remove aggregated Aβ deposited in the brains of AD patients with varied results (Agadjanyan et al., 2009; Agadjanyan et al., 2015; Bachmann, 2019; Delrieu et al., 2012; Ghochikyan and Agadjanyan, 2012; Godyn et al., 2016; Lemere and Masliah, 2010; Lobello et al., 2012; Panza et al., 2014; Selkoe, 2018; Wisniewski, 2009). Recent clinical trials data on humanized or fully human monoclonal antibodies (mAb) targeting oligomeric forms of Aβ suggest that such immunotherapy could clear/reduce brain amyloid plaques and slow cognitive decline in vaccinated subjects (Ostrowitzki et al., 2017; Panza et al., 2019; Panza et al., 2018; Salloway et al., 2018; Selkoe, 2018). For example, it was reported that amyloid plaques were cleared in 81% of subjects who received the highest dose of BAN2401 mAb, and cognitive decline was diminished in the cohort with “very mild or mild AD (Mini-Mental State Exam scores of 22–30) and positive amyloid PET scans” (Panza et al., 2019; Selkoe, 2018). These results are encouraging and indicate that therapeutically relevant concentrations of antibodies against Aβ oligomers could effectively delay/slow AD pathology if intervention was initiated early in disease manifestation. Previously it was reported that monthly injections of fully human mAb, aducanumab, decreased Aβ in the brain in a dose-dependent manner and slowed clinical decline (Sevigny et al., 2016 7905). However, Biogen announced the termination of the 3rd phase of aducanumab clinical trial in early Alzheimer's disease due to futility (Selkoe, 2019). The details of that trial have not yet been fully reported, but despite the efforts to recruit patients in the early stages of disease, most patients in the trail were too advanced in the disease to be able to benefit from the reduction of pathological Aβ. Recently, Biogen announced the results from expanded analyses (including an additional 3 months of data) on patients receiving high-dose aducanumab from the phase 3 EMERGE trial (Haeberlein et al., 2019) where a statistically significant improvement in the CDR-SB scores was found, as well as several other secondary endpoints.

Interestingly, our recent pre-clinical data on active vaccine targeting N-terminal B cell epitope of Aβ supported the clinical results obtained with mAb. More specifically, we reported that an immunogenic Aβ vaccine in a preventive setting, reduced the pathological forms of Aβ in the brains of Tg2576 mice, but in a therapeutic setting it induced low levels of antibodies that were not sufficient for clearance of AD-like pathology and improvement of cognitive functions (Petrushina et al., 2017). On the other hand, immunization of mice possessing pre-existing memory T cells specific to MultiTEP vaccine platform had quickly activated these memory T cells, had induced high titers of anti-Aβ antibodies, and improved cognitive functions in vaccinated mice. These data suggest that our AV-1959D vaccine can rapidly induce a robust anti-Aβ antibody production in vaccinated elderly individuals with pre-existing memory $CD4^+$ T cells that had been generated in response to conventional tetanus, hepatitis and flu vaccines and/or infections with these pathogens during the lifespan.

DNA vaccination exhibits properties that may be advantageous in developing of preventive vaccine against AD, as well as a variety of human diseases (Abdulhaqq and Weiner, 2008; Agadjanyan et al., 1998; Ghochikyan, 2009; Ghochikyan et al., 2003; Kim et al., 1998; Li et al., 2012; Lopes et al., 2019; Ugen et al., 2006). Specifically, DNA plasmids are relatively safe, cost- and time-efficient, and do not require conventional adjuvants that are frequently toxic. Although there are still no approved DNA vaccines for use in humans, some DNA-based vaccines were approved by the FDA and the USDA for veterinary use, and more importantly, more than 100 clinical trials with DNA vaccines targeting various cancers, infectious and autoimmune diseases have been conducted since the original DNA vaccine clinical trial almost two decades ago (Ferraro et al., 2011; Hobernik and Bros, 2018; Liu, 2011; Liu and Ulmer, 2005; Lopes et al., 2019). All DNA vaccines used so far were well tolerated with no local or systemic serious adverse effects (Bins et al., 2013; Ferraro et al., 2011; Schalk et al., 2006). However, it is known that DNA vaccines are relatively less effective in large animals and humans than in mice (Babiuk et al., 2003; Donnelly et al., 2005; Li et al., 2012). Thus, to improve in vivo uptake/expression of plasmid DNA and to induce robust immune responses in vaccinated subjects, an electroporation (EP) technology was used (Babiuk et al., 2002; Luxembourg et al., 2007; McCray et al., 2006; Roos et al., 2006; Sardesai and Weiner, 2011). Importantly, several EP devices, including the AgilePulse™ (aka DermaVax) used in this study, are currently being used in multiple Phase I-III clinical vaccine trials (Bagarazzi et al., 2012; Bodles-Brakhop et al., 2009; Chudley et al., 2012; Diehl et al., 2013; El-Kamary et al., 2012; Eriksson et al., 2013; Nilsson et al., 2015; van Drunen Littel-van den Hurk and Hannaman, 2010; Viegas et al., 2018).

Based on our preclinical safety data and in order to translate the AV-1959D vaccine into clinical trials for testing in a preventive setting, we generated cGMP grade product and analyzed its biodistribution and short-term and long-term safety profiles in Tg2576 mouse model. We also tested the acute neuropathological safety profile in CAA-prone Tg-SwDI mouse model of AD. Animal species for pre-clinical safety/toxicology studies were selected based on FDA recommendations. The FDA explicitly recommended that “Toxicity study is necessary to conduct in animal model where biological relevance has been established, such as Aβ plaque bearing transgenic (Tg) mice. Please note that at this time, we believe the use of healthy animals that do not develop pathological features of AD are of limited applicability in this study”.

In our biodistribution study, less than 100 copies of AV-1959D were detected in almost all organs and tissues examined, indicating a low rate of systemic migration of AV-1959D. High copy numbers of AV-1959D were detected at the injection sites, which persisted only in 25% of animals until 60 days post-injection, indicating fast clearance of AV-1959D even from injection sites. We observed some inter-individual variability in different tissues, mostly in male mice, although plasmid copy number was below 100 in all mice (except in two tissues of 1 mouse). This variability could be associated with the sex differences, although significant differences between sexes were not observed. High variability at the injection site could be associated with the skin tissue susceptibility to electrical pulses in individual mice. AV-1959D induced anti-Aβ antibodies in all vaccinated Tg2576 mice (Fig. 2) in this comparative evaluation study, and no acute or long-term toxicities were registered based on weekly clinical observations; daily general health observations; weekly body

weight measurements; full panel clinical pathology measurements (hematology, coagulation, clinical chemistry); terminal, gross necropsy observations; organ weights and histopathology examinations of all major organ systems and tissues.

Important issues observed in previous clinical trials with active and passive vaccines for AD were microhemorrhages, meningoencephalitis due to increased inflammation and lymphocyte infiltration of brain (Ferrer et al., 2004; Fox et al., 2005; Nicoll et al., 2003; Orgogozo et al., 2003), including vasogenic edema (Abushouk et al., 2017; Carlson et al., 2011; Kerchner and Boxer, 2010; Ostrowitzki et al., 2012; Sevigny et al., 2016). Thus we evaluated the potential of EP-mediated AV-1959D vaccination to provoke these side effects.

Edema, abnormal retention of water in the brain is often associated with adverse outcomes, clinically and in experimental models of neurological disease. While there are several invasive methods for assessing edema, non-invasive magnetic resonance imaging (MRI) can be utilized to monitor and quantify the presence and degree of edema present in brain tissues. Quantitative T2-weighted imaging (T2WI) can be used both to visualize and to quantify the amount of edema (Obenaus and Badaut, 2017) in severe neurological injury (i.e., stroke) and even in instances where no visible alterations increased water content can be identified (Rodriguez-Grande, 2018). Therefore, we analyzed vaccinated and control Tg-SwDI mice which show early-onset cerebral microvascular amyloidosis in the form of fibrillar vascular Aβ deposits (Davis et al., 2004; Davis et al., 2006; Vasilevko et al., 2007; Yang et al., 2011) by MRI. Data showed that vaccination did not significantly modify water content, brain size, or ventricular volumes in the brains of mice compared with PBS injected mice at 2 or 14 days after treatment (Fig. 4). No increase in the numbers of microhemorrhagic hypointensities was observed in vaccinated mice and confirmed by Prussian blue staining (Figs. 5-7). Thus, both invasive and non-invasive methods can be used to analyze edema and microhemorrhage which can monitor the safety aspects in live animals throughout a study.

One of the adverse events of anti-Aβ immunotherapy in AD patients can be CAA, which may develop due to rapid removal of parenchymal Aβ or triggered when exposed to antibodies against Aβ. We did not observe any increase in vascular deposition of Aβ in AV-1959D/EP vaccinated CAA-prone Tg-SwDI compared with control mice 2 or 14 days after the last immunization (Fig. 8).

Another important facet of AD is inflammation which plays a fundamental role in the disease progression, accelerating Aβ deposition, neuronal loss and cognitive impairment (Patel et al., 2005). Amyloid plaques in the brain invoke an intense phenotypic activation of the surrounding microglia (Herber et al., 2007). Microglia are brain tissue macrophages serving as the principal representatives of the innate immune system in the central nervous system (CNS). Microglia are the first line of defense in the brain, acting to protect the CNS from injury and pathogens by maintaining healthy tissue. They function by taking up and disposing of cellular debris in the brain parenchyma (Mandrekar-Colucci and Landreth, 2010), while expressing a variety of cell surface markers including the Iba1, CD11b, and MHC II (Ito et al., 1998). In AD brain tissues Aβ sustains chronic activation of primed microglia, constantly producing inflammatory cytokines and chemokines that impair

microglia, also affecting the surrounding CNS resident cells and possibly aggravating tau pathology that leads to neurodegeneration and loss of neurons. Based on our unpublished and published results, we expected that therapeutic vaccination would not reduce astrocyte activation significantly (although a slight decrease was observed), the goal of our current study was to ensure that vaccination does not enhance neuroinflammation. Therefore, we analyzed activated microglia and astrocytes, as well as leukocyte infiltration in the brains of vaccinated and control mice. No increases in astrocyte or microglia activation or infiltration of T and B cells were observed in AV-1959D/EP vaccinated mice compared to control animals 2 or 14 days after the last immunization (Figs. 8-10). Moreover, we observed a significant decrease in T cell infiltration in vaccinated mice at 14 days after the last immunization (Fig. 10). No differences were observed in numbers of necrotic/apoptotic cells in vaccinated and control mice (Fig. 11). Importantly, we concluded that the AV-1959D vaccine did not increase inflammation associated with Aβ pathology known to be present in aged Tg-SwDI mice.

5. Conclusion

We manufactured GMP-grade DNA vaccine AV-1959D, completed IND-enabling biodistribution/persistence, acute and long-term safety/toxicology studies, and found that the vaccine has a favorable safety profile. We observed no short- or long-term toxicities in Tg2576 mice that would preclude approval of an IND for AV-1959D trials. An assessment of the repeat dose acute safety of AV-1959D in CAA-prone Tg-SwDI mice did not reveal any immunotherapy-induced (i) vasogenic edema detected by magnetic resonance imaging (MRI); (ii) increase in microhemorrhages, T and B cell infiltration, glial activation, vascular deposition of Aβ and neuronal degeneration (necrosis and apoptosis) greater than that in control mice determined by immunohistochemistry/histochemistry of brain tissues.

Funding

This work was supported by the National Institutes of Health (NIA grant 5UO1 AG048310-04).

References

Abdulhaqq SA, Weiner DB, 2008. DNA vaccines: developing new strategies to enhance immune responses. Immunol. Res 42, 219–232. [PubMed: 19066740]

Abushouk AI, et al. , 2017. Bapineuzumab for mild to moderate Alzheimer's disease: a meta-analysis of randomized controlled trials. BMC Neurol. 17, 66. [PubMed: 28376794]

Agadjanyan MG, et al. , 1998. DNA plasmid based vaccination against the oncogenic human T cell leukemia virus type 1. Curr. Top. Microbiol. Immunol 226, 175–192. [PubMed: 9479842]

Agadjanyan MG, et al. , 2005. Prototype Alzheimer's disease vaccine using the immunodominant B cell epitope from beta-amyloid and promiscuous T cell epitope pan HLA DR-binding peptide. J. Immunol 174, 1580–1586. [PubMed: 15661919]

Agadjanyan M, et al. , 2009. Active and passive Aβ-immunotherapy: positive and negative outcomes from pre-clinical and clinical trials and future directions. CNS Neurol. Disord. Drug Targets 8.

Agadjanyan MG, et al. , 2015. A fresh perspective from immunologists and vaccine researchers: active vaccination strategies to prevent and reverse Alzheimer's disease. Alzheimers Dement. 11, 1246–1259. [PubMed: 26192465]

Arai H, et al. , 2015. Vanutide Cridificar and the QS-21 adjuvant in Japanese subjects with mild to moderate Alzheimer's disease: results from two phase 2 studies. Curr. Alzheimer Res 12, 242–254. [PubMed: 25731629]

Babiuk S, et al. , 2002. Electroporation improves the efficacy of DNA vaccines in large animals. Vaccine. 20, 3399–3408. [PubMed: 12213410]

Babiuk LA, et al. , 2003. Induction of immune responses by DNA vaccines in large animals. Vaccine. 21, 649–658. [PubMed: 12531334]

Bachmann MF, et al. , 2019. A vaccine against Alzheimer's disease: anything left but faith? Expert. Opin. Biol. Ther 19 (1), 73–78. [PubMed: 30526133]

Bagarazzi ML, et al. , 2012. Immunotherapy against HPV16/18 generates potent TH1 and cytotoxic cellular immune responses. Sci. Transl. Med 4 155ra138.

Baghchechi M, et al. , 2016. Susceptibility-weighted imaging identifies iron-oxide-labeled human neural stem cells: automated computational detection. Dev. Neurosci 38 (6), 445–457. 10.1159/000455837. 28343216. [PubMed: 28343216]

Bins AD, et al. , 2013. Recent advances towards the clinical application of DNA vaccines. Neth. J. Med 71, 109–117. [PubMed: 23712805]

Boche D, et al. , 2008. Consequence of Abeta immunization on the vasculature of human Alzheimer's disease brain. Brain. 131, 3299–3310. [PubMed: 18953056]

Bodles-Brakhop AM, et al. , 2009. Electroporation for the delivery of DNA-based vaccines and immunotherapeutics: current clinical developments. Mol. Ther 17, 585–592. [PubMed: 19223870]

Carlson C, et al. , 2011. Prevalence of asymptomatic vasogenic edema in pretreatment Alzheimer's disease study cohorts from phase 3 trials of semagacestat and solanezumab. Alzheimers Dement. 7, 396–401. [PubMed: 21784350]

Chudley L, et al. , 2012. DNA fusion-gene vaccination in patients with prostate cancer induces high-frequency CD8(+) T-cell responses and increases PSA doubling time. Cancer Immunol. Immunother 61, 2161–2170. [PubMed: 22729556]

Cleary JP, et al. , 2005. Natural oligomers of the amyloid-beta protein specifically disrupt cognitive function. Nat. Neurosci 8, 79–84. [PubMed: 15608634]

Cline EN, et al. , 2018. The amyloid-beta oligomer hypothesis: beginning of the third decade. J. Alzheimers Dis 64, S567–S610. [PubMed: 29843241]

Davis J, et al. , 2004. Early-onset and robust cerebral microvascular accumulation of amyloid beta-protein in transgenic mice expressing low levels of a vasculotropic Dutch/Iowa mutant form of amyloid beta-protein precursor. J. Biol. Chem 279, 20296–20306. [PubMed: 14985348]

Davis J, et al. , 2006. Deficient cerebral clearance of vasculotropic mutant Dutch/Iowa double a beta in human a betaPP transgenic mice. Neurobiol. Aging 27, 946–954. [PubMed: 16105708]

Davtyan H, et al. , 2010. DNA prime-protein boost increased the titer, avidity and persistence of anti-Abeta antibodies in wild-type mice. Gene Ther. 17, 261–271. [PubMed: 19865176]

Davtyan H, et al. , 2013. Immunogenicity, efficacy, safety, and mechanism of action of epitope vaccine (Lu AF20513) for Alzheimer's disease: prelude to a clinical trial. J. Neurosci 33, 4923–4934. [PubMed: 23486963]

Davtyan H, et al. , 2014a. The MultiTEP platform-based Alzheimer's disease epitope vaccine activates a broad repertoire of T helper cells in nonhuman primates. Alzheimers Dement. 10, 271–283. [PubMed: 24560029]

Davtyan H, et al. , 2014b. BTX AgilePulse(TM) system is an effective electroporation device for intramuscular and intradermal delivery of DNA vaccine. Curr. Gene. Ther 14, 190–199. [PubMed: 24867066]

Delrieu J, et al. , 2012. Clinical trials in Alzheimer's disease': immunotherapy approaches. J. Neurochem 120 (Suppl. 1), 186–193. [PubMed: 21883222]

Derhovanessian E, et al. , 2008. Immunity, ageing and cancer. Immun. Ageing 5, 11. [PubMed: 18816370]

Diehl MC, et al. , 2013. Tolerability of intramuscular and intradermal delivery by CELLECTRA((R)) adaptive constant current electroporation device in healthy volunteers. Hum. Vaccin Immunother 9, 2246–2252. [PubMed: 24051434]

Donnelly JJ, et al. , 2005. DNA vaccines: progress and challenges. J. Immunol 175, 633–639. [PubMed: 16002657]

El-Kamary SS, et al. , 2012. Safety and tolerability of the easy vax clinical epidermal electroporation system in healthy adults. Mol. Ther 20, 214–220. [PubMed: 22068424]

Eriksson F, et al. , 2013. DNA vaccine coding for the rhesus prostate specific antigen delivered by intradermal electroporation in patients with relapsed prostate cancer. Vaccine. 31, 3843–3848. [PubMed: 23831327]

Evans CF, et al. , 2014. Epitope-based DNA vaccine for Alzheimer's disease: translational study in macaques. Alzheimers Dement. 10, 284–295. [PubMed: 23916838]

FDA, 1996. Points to Consider on Plasmid DNA Vaccines for Preventive Infectious Diseases Indications. In: C. f. B. E. a. R. (CBER), (Ed.), Docket no. 96N–0400. .

FDA, 2007. Guidance for Industry: Considerations for Plasmid DNA Vaccines for Infectious Disease Indications.

Ferraro B, et al. , 2011. Clinical applications of DNA vaccines: current progress. Clin. Infect. Dis 53, 296–302. [PubMed: 21765081]

Ferrer I, et al. , 2004. Neuropathology and pathogenesis of encephalitis following amyloid-beta immunization in Alzheimer's disease. Brain Pathol. 14, 11–20. [PubMed: 14997933]

Fox NC, et al. , 2005. Effects of Abeta immunization (AN1792) on MRI measures of cerebral volume in Alzheimer disease. Neurology. 64, 1563–1572. [PubMed: 15883317]

Ghochikyan A, 2009. Rationale for peptide and DNA based epitope vaccines for Alzheimer's disease immunotherapy. CNS Neurol. Disord. Drug Targets 8, 128–143. [PubMed: 19355933]

Ghochikyan A, Agadjanyan MG, 2012. CAD-106, a beta-amyloid-based immunotherapeutic for Alzheimer's disease. Thompson Reuter. https://partnering.thomson-pharma.com.

Ghochikyan A, et al. , 2003. Generation and chracterization of the humoral immune response to DNA immunization with a chimeric b-amyloid-interleukin-4 minigene. Eur. J. Immunol 33, 3232–3241. [PubMed: 14635031]

Ghochikyan A, et al. , 2006. Prototype Alzheimer's disease epitope vaccine induced strong Th2-type anti-Abeta antibody response with alum to Quil a adjuvant switch. Vaccine. 24, 2275–2282. [PubMed: 16368167]

Ghochikyan A, et al. , 2013. Refinement of a DNA based Alzheimer's disease epitope vaccine in rabbits. Hum. Vaccin. Immunother 9, 1002–1010. [PubMed: 23399748]

Ghosh N, et al. , 2012. Automated core-penumbra quantification in neonatal ischemic brain injury. J. Cereb. Blood Flow Metab 32, 2161–2170. [PubMed: 22929436]

Gilman S, et al. , 2005. Clinical effects of Abeta immunization (AN1792) in patients with AD in AN interrupted trial. Neurology. 64, 1553–1562. [PubMed: 15883316]

Godyn J, et al. , 2016. Therapeutic strategies for Alzheimer's disease in clinical trials. Pharmacol. Rep 68, 127–138. [PubMed: 26721364]

Golde TE, et al. , 2006. Filling the gaps in the abeta cascade hypothesis of Alzheimer's disease. Curr. Alzheimer Res. 3, 421–430. [PubMed: 17168641]

Haass C, Selkoe DJ, 2007. Soluble protein oligomers in neurodegeneration: lessons from the Alzheimer's amyloid beta-peptide. Nat. Rev. Mol. Cell Biol 8, 101–112. [PubMed: 17245412]

Haeberlein SB, et al., 2019. EMERGE and ENGAGE Topline Results: Two Phase 3 Studies to Evaluate Aducanumab in Patients With Early Alzheimer's Disease. 12th Clinical Trials on Alzheimer's Disease (CTAD) Congress, San Diego, CA.

Hardy J, 2006. Has the amyloid cascade hypothesis for Alzheimer's disease been proved? Curr. Alzheimer Res 3, 71–73. [PubMed: 16472206]

Hardy JA, Higgins GA, 1992. Alzheimer's disease: the amyloid cascade hypothesis. Science. 256, 184–185. [PubMed: 1566067]

Herber DL, et al. , 2007. Microglial activation is required for Abeta clearance after intracranial injection of lipopolysaccharide in APP transgenic mice. J. NeuroImmune Pharmacol 2, 222–231. [PubMed: 18040847]

Hobernik D, Bros M, 2018. DNA vaccines-how far from clinical use? Int. J. Mol. Sci 19.

Holmes C, et al. , 2008. Long-term effects of Abeta42 immunization in Alzheimer's disease: follow-up of a randomised, placebo-controlled phase I trial. Lancet. 372, 216–223. [PubMed: 18640458]

Ito D, et al. , 1998. Microglia-specific localisation of a novel calcium binding protein, Iba1. Brain Res. Mol. Brain Res 57, 1–9. [PubMed: 9630473]

Kerchner GA, Boxer AL, 2010. Bapineuzumab. Expert. Opin. Biol. Ther 10, 1121–1130. [PubMed: 20497044]

Kim JJ, et al. , 1998. Engineering DNA vaccines via co-delivery of co-stimulatory molecule genes. Vaccine. 16, 1828–1835. [PubMed: 9795388]

Klein WL, et al. , 2004. Small assemblies of unmodified amyloid beta-protein are the proximate neurotoxin in Alzheimer's disease. Neurobiol. Aging 25, 569–580. [PubMed: 15172732]

Klohs J, et al. , 2014. Imaging of cerebrovascular pathology in animal models of Alzheimer's disease. Front. Aging Neurosci 6, 32. [PubMed: 24659966]

Kruyer A, et al. , 2015. Chronic hypertension leads to neurodegeneration in the TgSwDI mouse model of Alzheimer's disease. Hypertension. 66, 175–182. [PubMed: 25941345]

Lacor PN, et al. , 2007. Abeta oligomer-induced aberrations in synapse composition, shape, and density provide a molecular basis for loss of connectivity in Alzheimer's disease. J. Neurosci 27, 796–807. [PubMed: 17251419]

Lambert MP, et al. , 1998. Diffusible, nonfibrillar ligands derived from Abeta1-42 are potent central nervous system neurotoxins. Proc. Natl. Acad. Sci. U. S. A 95, 6448–6453. [PubMed: 9600986]

Lemere CA, Masliah E, 2010. Can Alzheimer disease be prevented by amyloid-beta immunotherapy? Nat. Rev. Neurol 6, 108–119. [PubMed: 20140000]

Li L, et al. , 2012. The future of human DNA vaccines. J. Biotechnol 162, 171–182. [PubMed: 22981627]

Liu MA, 2011. DNA vaccines: an historical perspective and view to the future. Immunol. Rev 239, 62–84. [PubMed: 21198665]

Liu MA, Ulmer JB, 2005. Human clinical trials of plasmid DNA vaccines. Adv. Genet 55, 25–40. [PubMed: 16291211]

Lobello K, et al. , 2012. Targeting Beta amyloid: a clinical review of immunotherapeutic approaches in Alzheimer's disease. Int. J. Alzheimers Dis 2012, 628070. [PubMed: 22292124]

Lopes A, et al. , 2019. Cancer DNA vaccines: current preclinical and clinical developments and future perspectives. J. Exp. Clin. Cancer Res. 38, 146.

Luxembourg A, et al. , 2007. Electroporation-based DNA immunisation: translation to the clinic. Expert. Opin. Biol. Ther 7, 1647–1664. [PubMed: 17961089]

Mandrekar-Colucci S, Landreth GE, 2010. Microglia and inflammation in Alzheimer's disease. CNS Neurol. Disord. Drug Targets 9, 156–167. [PubMed: 20205644]

Marciani DJ, 2016. A retrospective analysis of the Alzheimer's disease vaccine progress - the critical need for new development strategies. J. Neurochem 137, 687–700. [PubMed: 26990863]

McCray AN, et al. , 2006. Complete regression of established subcutaneous B16 murine melanoma tumors after delivery of an HIV-1 Vpr-expressing plasmid by in vivo electroporation. Mol. Ther 14, 647–655. [PubMed: 16950655]

Miao J, et al. , 2005a. Reducing cerebral microvascular amyloid-beta protein deposition diminishes regional neuroinflammation in vasculotropic mutant amyloid precursor protein transgenic mice. J. Neurosci 25, 6271–6277. [PubMed: 16000616]

Miao J, et al. , 2005b. Cerebral microvascular amyloid beta protein deposition induces vascular degeneration and neuroinflammation in transgenic mice expressing human vasculotropic mutant amyloid beta precursor protein. Am. J. Pathol 167, 505–515. [PubMed: 16049335]

Movsesyan N, et al. , 2008a. Reducing AD-like pathology in 3xTg-AD mouse model by DNA epitope vaccine- a novel immunotherapeutic strategy. PLoS One 3, e21–e24.

Movsesyan N, et al. , 2008b. DNA epitope vaccine containing complement component C3d enhances anti-amyloid-beta antibody production and polarizes the immune response towards a Th2 phenotype. J. Neuroimmunol 205, 57–63. [PubMed: 18838175]

Neurimmune, 2015. Aducanumab (BIIB037) reduced brain amyloid plaque levels and slowed cognitive decline in patients with prodromal or mild Alzheimer's disease in Phase 1b study. Biogen IDEC presents positive interim results from Phase 1b study at 2015 AD/PD conference.

Nicoll JA, et al. , 2003. Neuropathology of human Alzheimer disease after immunization with amyloid-beta peptide: a case report. Nat. Med 9, 448–452. [PubMed: 12640446]

Nicoll JA, et al. , 2006. Abeta species removal after abeta42 immunization. J. Neuropathol. Exp. Neurol 65, 1040–1048. [PubMed: 17086100]

Nilsson C, et al. , 2015. HIV-DNA given with or without intradermal electroporation is safe and highly immunogenic in healthy Swedish HIV-1 DNA/MVA Vaccinees: a phase I randomized trial. PLoS One 10, e0131748. [PubMed: 26121679]

Obenaus A, Badaut J, 2017. Neuroimaging of brain Edema. In: Badaut J, Plesnila N (Eds.), Brain Edema: From Molecular Mechanisms to Clinical Practice. Elsevier, Inc.

Obenaus A, et al. , 2017. Traumatic brain injury results in acute rarefication of the vascular network. Sci. Rep 7, 239. [PubMed: 28331228]

Orgogozo JM, et al. , 2003. Subacute meningoencephalitis in a subset of patients with AD after Abeta42 immunization. Neurology. 61 (1), 46–54. [PubMed: 12847155]

Ostrowitzki S, et al. , 2012. Mechanism of amyloid removal in patients with Alzheimer disease treated with gantenerumab. Arch. Neurol 69, 198–207. [PubMed: 21987394]

Ostrowitzki S, et al. , 2017. A phase III randomized trial of gantenerumab in prodromal Alzheimer's disease. Alzheimers Res. Ther 9, 95. [PubMed: 29221491]

Panza F, et al. , 2014. Amyloid-based immunotherapy for Alzheimer's disease in the time of prevention trials: the way forward. Expert. Rev. Clin. Immunol 10, 405–419. [PubMed: 24490853]

Panza F, et al. , 2018. The potential of solanezumab and gantenerumab to prevent Alzheimer's disease in people with inherited mutations that cause its early onset. Expert. Opin. Biol. Ther 18, 25–35. [PubMed: 29037101]

Panza F, et al. , 2019. Are antibodies directed against amyloid-beta (Abeta) oligomers the last call for the Abeta hypothesis of Alzheimer's disease? Immunotherapy. 11, 3–6. [PubMed: 30702009]

Passos GF, et al. , 2013. The bradykinin B1 receptor regulates Abeta deposition and neuroinflammation in Tg-SwDI mice. Am. J. Pathol 182, 1740–1749. [PubMed: 23470163]

Patel NS, et al. , 2005. Inflammatory cytokine levels correlate with amyloid load in transgenic mouse models of Alzheimer's disease. J. Neuroinflammation 2, 9. [PubMed: 15762998]

Petrushina I, et al. , 2007. Alzheimer's disease peptide epitope vaccine reduces insoluble but not soluble/oligomeric A{beta} species in amyloid precursor protein transgenic mice. J. Neurosci 27, 12721–12731. [PubMed: 18003852]

Petrushina I, et al. , 2017. Comparison of efficacy of preventive and therapeutic vaccines targeting the N terminus of beta-amyloid in an animal model of Alzheimer's disease. Mol. Ther 25, 153–164. [PubMed: 28129111]

Rodriguez-Grande B, et al. , 2018. Gliovascular changes precede white matter damage and long-term disorders in juvenile mild closed head injury. Glia. 66 (8), 1663–1677. 10.1002/glia.23336.29665077. [PubMed: 29665077]

Roos AK, et al. , 2006. Enhancement of cellular immune response to a prostate cancer DNA vaccine by intradermal electroporation. Mol. Ther 13, 320–327. [PubMed: 16185933]

Ryan JM, Grundman M, 2009. Anti-amyloid-beta immunotherapy in Alzheimer's disease: ACC-001 clinical trials are ongoing. J. Alzheimers Dis 17, 243. [PubMed: 19502708]

Salloway S, et al. , 2018. Amyloid positron emission tomography and cerebrospinal fluid results from a crenezumab anti-amyloid-beta antibody double-blind, placebo-controlled, randomized phase II study in mild-to-moderate Alzheimer's disease (BLAZE). Alzheimers Res. Ther 10, 96. [PubMed: 30231896]

Sardesai NY, Weiner DB, 2011. Electroporation delivery of DNA vaccines: prospects for success. Curr. Opin. Immunol 23, 421–429. [PubMed: 21530212]

Schalk JA, et al. , 2006. Preclinical and clinical safety studies on DNA vaccines. Hum. Vaccin 2, 45–53. [PubMed: 17012886]

Schneeberger A, et al. , 2010. AFFITOME(R) technology in neurodegenerative diseases: the doubling advantage. Hum. Vaccin 6, 948–952. [PubMed: 20980801]

Selkoe DJ, 1991. The molecular pathology of Alzheimer's disease. Neuron. 6, 487–498. [PubMed: 1673054]

Selkoe DJ, 1994. Alzheimer's disease: a central role for amyloid. J. Neuropathol. Exp. Neurol 53, 438–447. [PubMed: 8083687]

Selkoe DJ, 2018. Light at the end of the amyloid TunnelPublished as part of the biochemistry series "biochemistry to bedside". Biochemistry. 57, 5921–5922. [PubMed: 30272957]

Selkoe DJ, 2019. Alzheimer disease and aducanumab: adjusting our approach. Nat. Rev. Neurol 15, 365–366. [PubMed: 31138932]

Sevigny J, et al. , 2016. The antibody aducanumab reduces Abeta plaques in Alzheimer's disease. Nature. 537, 50–56. [PubMed: 27582220]

Shankar GM, et al. , 2007. Natural oligomers of the Alzheimer amyloid-beta protein induce reversible synapse loss by modulating an NMDA-type glutamate receptor-dependent signaling pathway. J. Neurosci 27, 2866–2875. [PubMed: 17360908]

Shankar GM, et al. , 2008. Amyloid-beta protein dimers isolated directly from Alzheimer's brains impair synaptic plasticity and memory. Nat. Med 14, 837–842. [PubMed: 18568035]

Smith LM, Strittmatter SM, 2017. Binding sites for amyloid-beta oligomers and synaptic toxicity. Cold Spring Harb Perspect Med. 7.

Spencer B, Masliah E, 2014. Immunotherapy for Alzheimer's disease: past, present and future. Front. Aging Neurosci 6, 114. [PubMed: 24959143]

Ugen KE, et al. , 2006. Regression of subcutaneous B16 melanoma tumors after intratumoral delivery of an IL-15-expressing plasmid followed by in vivo electroporation. Cancer Gene Ther 13, 969–974. [PubMed: 16763607]

van Drunen Littel-Van den Hurk S, Hannaman D, 2010. Electroporation for DNA immunization: clinical application. Expert Rev. Vaccines 9, 503–517. [PubMed: 20450325]

Vasilevko V, et al. , 2007. Experimental investigation of antibody-mediated clearance mechanisms of amyloid-beta in CNS of Tg-SwDI transgenic mice. J. Neurosci 27, 13376–13383. [PubMed: 18057195]

Viegas EO, et al. , 2018. Optimizing the immunogenicity of HIV prime-boost DNA-MVA-rgp140/GLA vaccines in a phase II randomized factorial trial design. PLoS One 13, e0206838. [PubMed: 30496299]

Wang CY, et al. , 2007. Site-specific UBITh amyloid-beta vaccine for immunotherapy of Alzheimer's disease. Vaccine. 25, 3041–3052. [PubMed: 17287052]

Wang CY, et al. , 2017. UB-311, a novel UBITh((R)) amyloid beta peptide vaccine for mild Alzheimer's disease. Alzheimers Dement (N Y). 3, 262–272. [PubMed: 29067332]

Winblad BG, et al. , 2009. Results of the first-in-man study with the active Abeta immunotherapy CAD106 in Alzheimer's patients. Alzheimers Dement (N Y) 5, 113–114.

Winblad B, et al. , 2012. Safety, tolerability, and antibody response of active Abeta immunotherapy with CAD106 in patients with Alzheimer's disease: randomised, double-blind, placebo-controlled, first-in-human study. Lancet Neurol. 11, 597–604. [PubMed: 22677258]

Wisniewski T, 2009. AD vaccines: conclusions and future directions. CNS Neurol. Disord. Drug Targets 8, 160–166. [PubMed: 19355935]

Yang J, et al. , 2011. Blocking the apolipoprotein E/amyloid-beta interaction reduces fibrillar vascular amyloid deposition and cerebral microhemorrhages in TgSwDI mice. J. Alzheimers Dis 24, 269–285. [PubMed: 21239853]

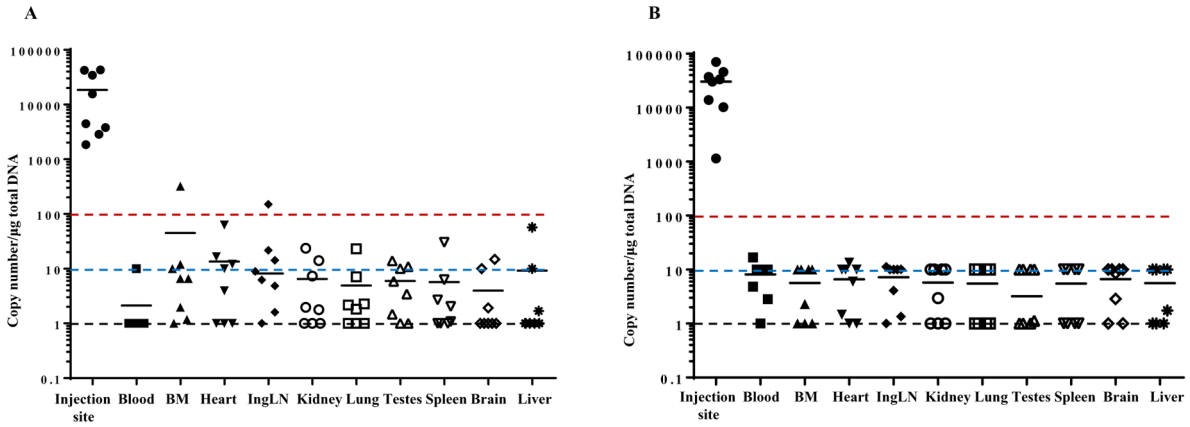

Fig. 1.

Biodistribution of AV-1959D followed by EP-mediated single administration in male (A) and female (B) Tg2576 mice. Tissue samples were taken and processed 2 days after the single administration. Plasmid copy numbers were determined by qPCR. Primers and probe were designed to detect 76 bp sequence present in AV-1959D plasmid in the region encoding MultiTEP. Individual animal data and geometric mean values are provided in a log scale. The black dotted line indicates the limit of detection, LOD. The blue dotted line indicates the limit of quantification LOQ of qPCR assay performed in this study. The red dotted line indicates the LOQ required by FDA (FDA, 2007) and the upper limit, which does not require testing of the plasmid persistence at the later point.

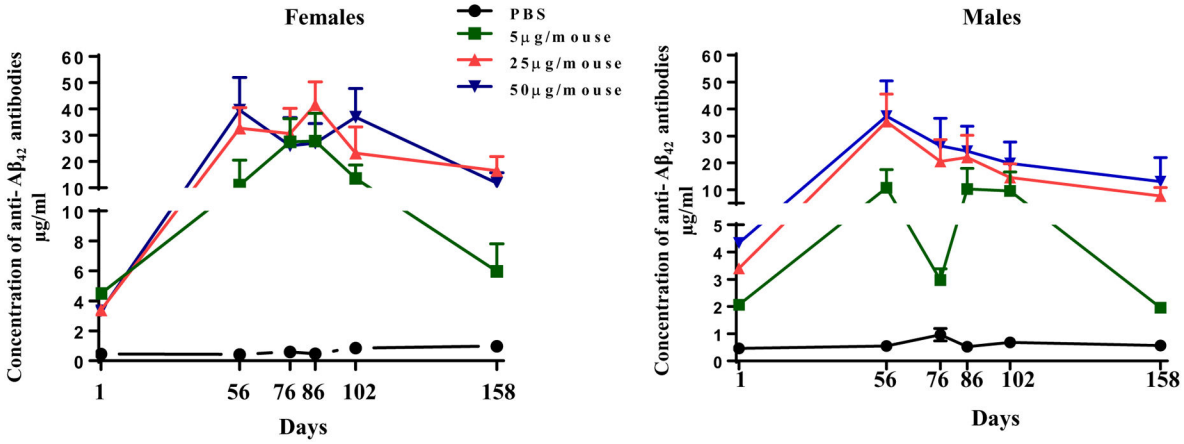

Fig. 2.

Dynamics of humoral immune responses in Tg2576 mice vaccinated with AV-1959D/EP at doses of 5 μg/mouse (*n* = 10F/10M), 25 μg/mouse (n = 10F/10M) and 50 μg/mouse (n = 10F/10M) or injected with PBS (n = 10F/10M) for our acute and long-term safety/toxicology study. Sera were collected 14 days after the third (on Day 56) and the fourth (on Day 86) immunizations, as well as at sacrificial end-points (Days 76, 102 and 158). Concentrations of anti-Aβ antibodies were determined by ELISA as described in Materials and Methods and calculated using a calibration curve generated with 6E10 monoclonal antibody. Each point represents the mean value of antibody concentration (average ± SEM) in a group (n = 10).

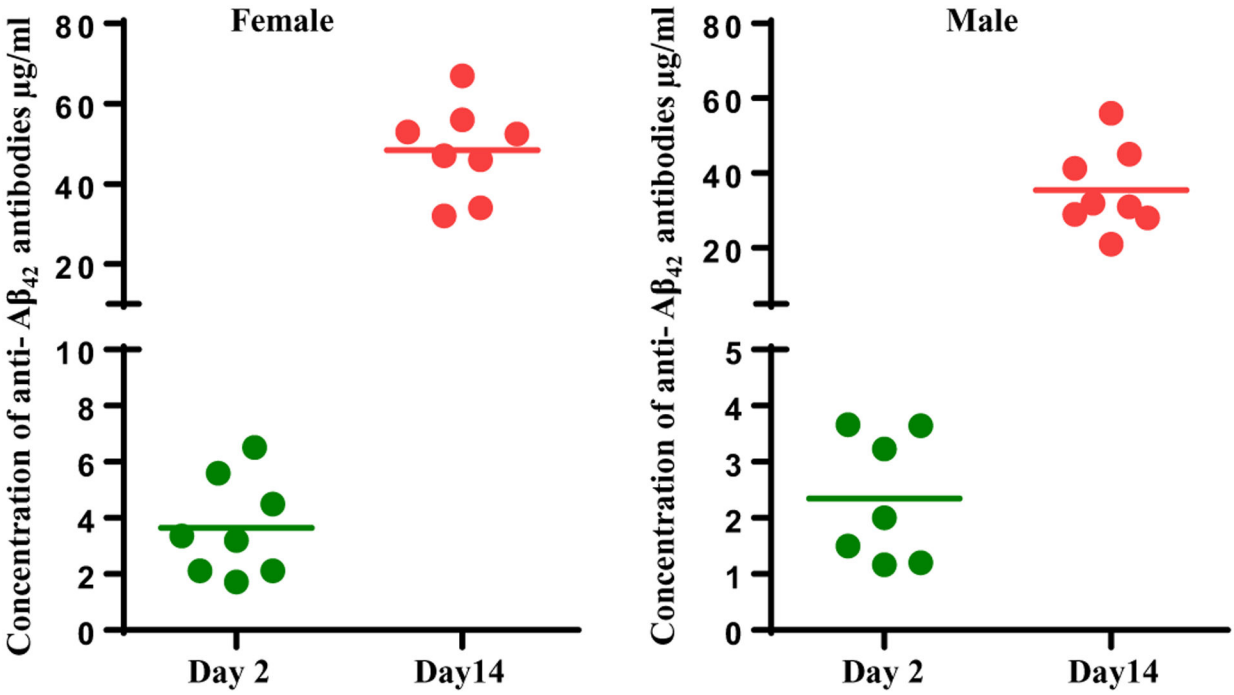

Fig. 3.

AV-1959D vaccinations generated humoral immune responses in all Tg-SwD/I mice. Concentrations of anti-Aβ antibodies in vaccinated male and female mice on Day 2 (*n* = 8F/8M) and Day 14 (n = 8F/7M) after the last immunization were determined by ELISA as described in Materials and Methods and calculated using a calibration curve generated with 6E10 monoclonal antibody. The lines represent mean values of antibody concentrations.

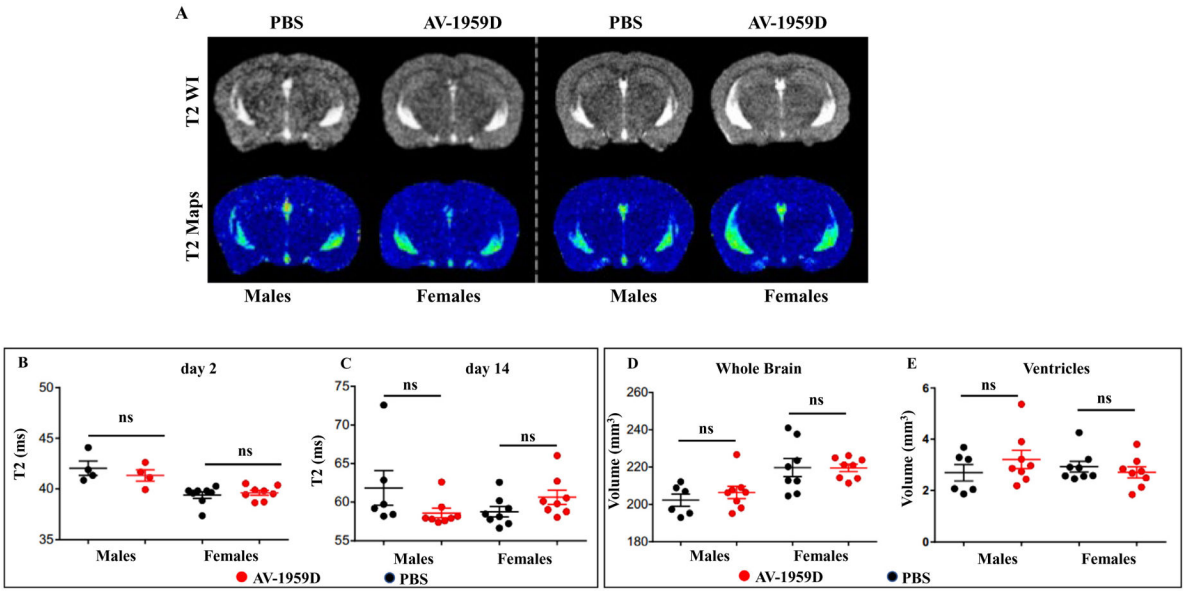

Fig. 4.

No vasogenic edema was detected by magnetic resonance imaging (MRI) in control and vaccinated Tg-SwD/I mice. (A) Representative T2WI and T2 Map images from males/females and control/immunized Tg-SwDI mice (n = 8/group) at day 2 immunization. No overt increases in edema were observed visually. (B) No significant changes in edema (T2 values) were observed among experimental groups at day 2 immunization. (C) At day 14 post immunotherapy, there were no significant differences between control and immunized males. (D) Whole-brain volumes were also assessed, and while no differences in brain volume were found between control and immunized groups (either males or females), control males had significantly smaller brain volumes than females (control and immunized) (two-way ANOVA, Tukey's multiple comparisons, $*p < .05$). (E) Similarly, ventricular volumes (3rd, 4th ventricles) were also quantified, but no significant differences between male and female, nor control vs. immunized mice were observed (two-way ANOVA, Tukey's multiple comparisons).

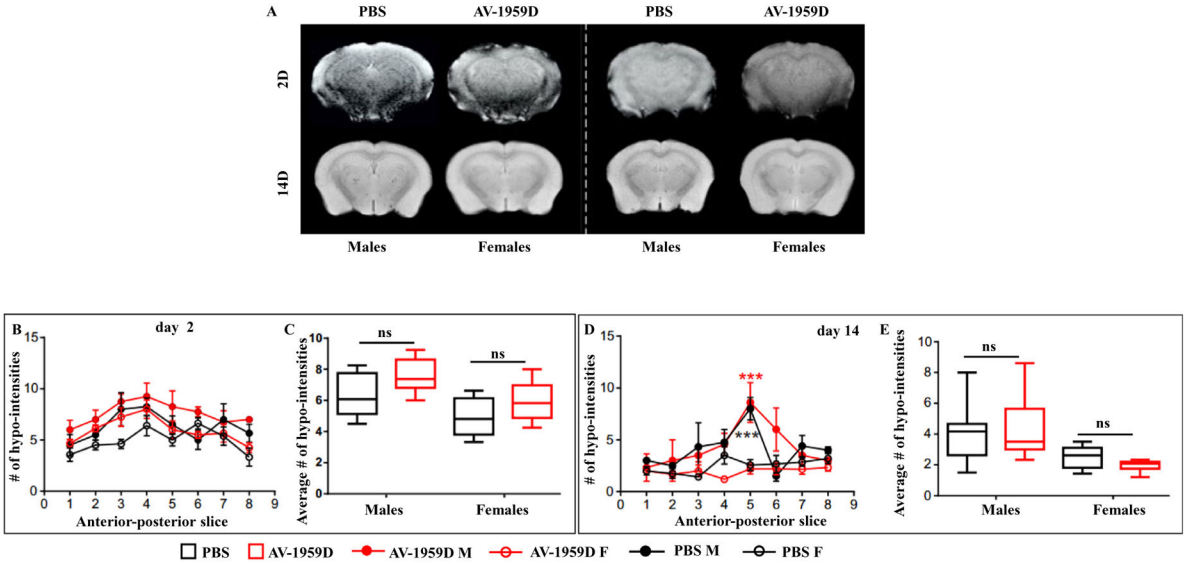

Fig. 5.

SWI hypointensities. (A) Representative SWI images at days 2 and 14 posttreatment in male/female and control/immunized Tg-SwDI mice (n = 8/group). No differences were apparent visually. (B) Anterior-posterior quantification of the SWI hypo-intensities at day 2 post-immunization revealed no significant differences between male and female groups (two-way ANOVA, Tukey's multiple comparisons). C) The average number of hypo-intensities over the whole brain was assessed at day 2 within the brains of treated Tg-SwDI mice and did not differ among groups. (D) There were no significant differences in SWI hypo-intensities at day 14 post-immunization in males and females. However, both control and immunized males at the level of the dorsal hippocampus had significantly increased hypo-intensities (slice 5) compared to control and immunized females (two-way ANOVA, Tukey's multiple comparisons, ***$p < .001$). E) When the average numbers of hypo-intensities were evaluated at day 14 after treatment across all MRI slices, no significant differences were observed, n = 8/group.

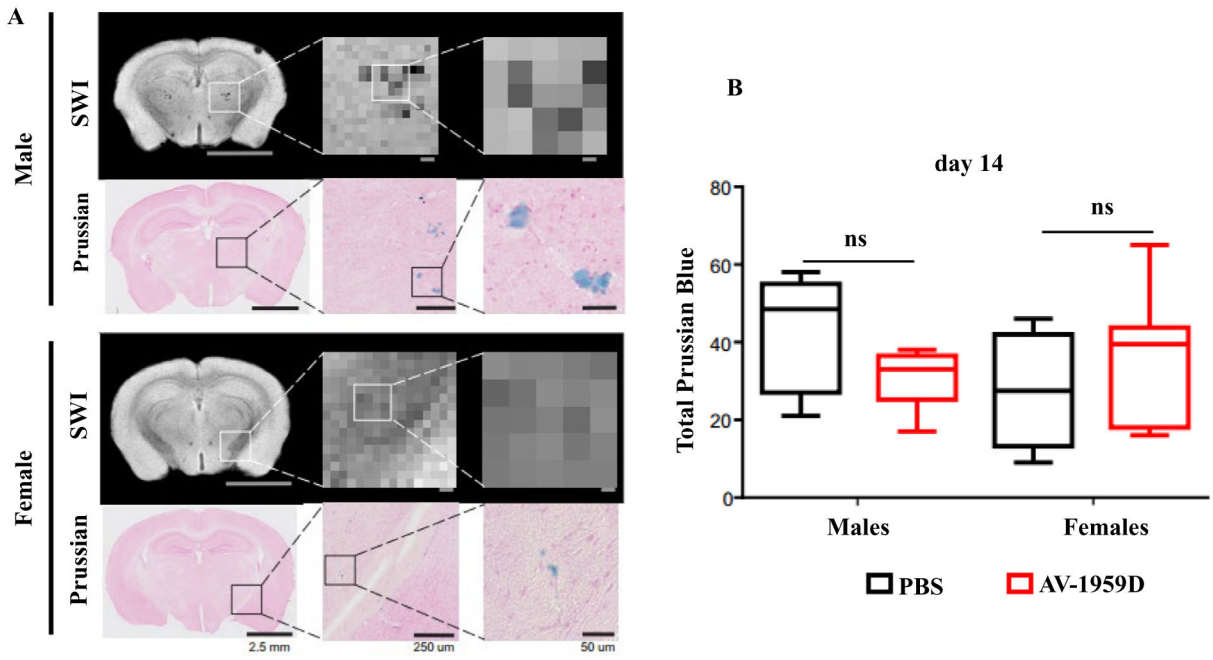

Fig. 6.

Prussian blue comparisons to SWI hypo-intensities. (A) Representative SWI and Prussian Blue images at day 14. Increased magnification of the original SWI and Prussian Blue images (1.25, 10 and 20 ×) illustrate the appearance of numerous hypo-intensities and Prussian Blue puncta and aggregates. The signal loss (dark gray, black pixels) in the SWI MRI images as a result of iron deposition was confirmed by the high-magnification Prussian Blue histology. The locations of the SWI and the positive Prussian Blue profiles overlapped reasonably well. Histological sections have considerably higher densities of Prussian Blue compared to SWI due to micron vs. mm resolution. As in Fig. 5, males at the level of dorsal hippocampus had increased hypo-intensities and the appearance of increased numbers and larger size of puncta and aggregates, and Prussian Blue staining confirmed these findings. Females tended to have fewer and smaller hypo-intensities and Prussian Blue staining puncta. Data shown are from SWI minimum intensity projections. Male and female mice shown are from control Tg-SwDI mice, and immunized mice showed very similar patterns. (B) Summation of all Prussian Blue puncta observed on 3 histological sections spanning the MRI slice confirmed no significant differences between any of the experimental groups at day 14 post-immunization.

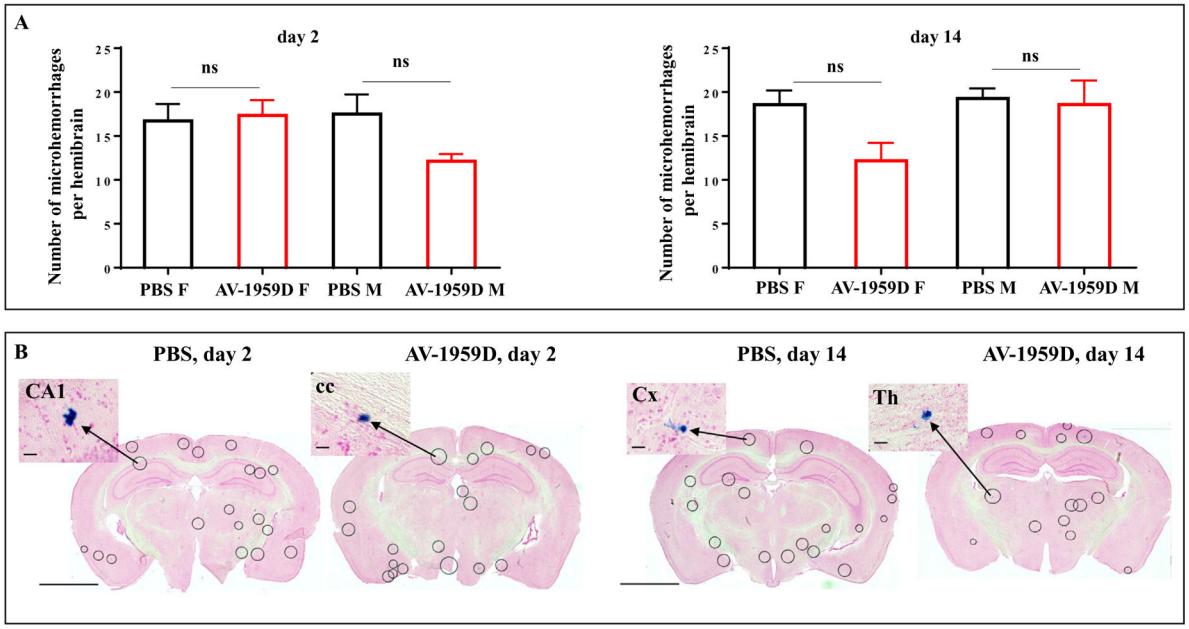

Fig. 7.

Number of microhemorrhages in the brains of Tg-SwDI mice vaccinated with AV-1959D. (A) No differences in the number of microhemorrhage profiles in mice were ben detected between control (*n* = 7/gender/time point) and vaccinated animals (n = 8/gender/time point) terminated at days 2 and 14 after the last immunization. Bars represent average ± SEM. (B) Photomicrographs show representative images of the coronal brain sections of immunized and control mice stained with Prussian Blue. Encircled areas indicate Prussian Blue profiles in CA1 (field CA1 of hippocampus), cc (corpus callosum), Cx (cortex), Th (thalamus). Scale bars: low magnification =2.5 mm, enlarged images =100 μm

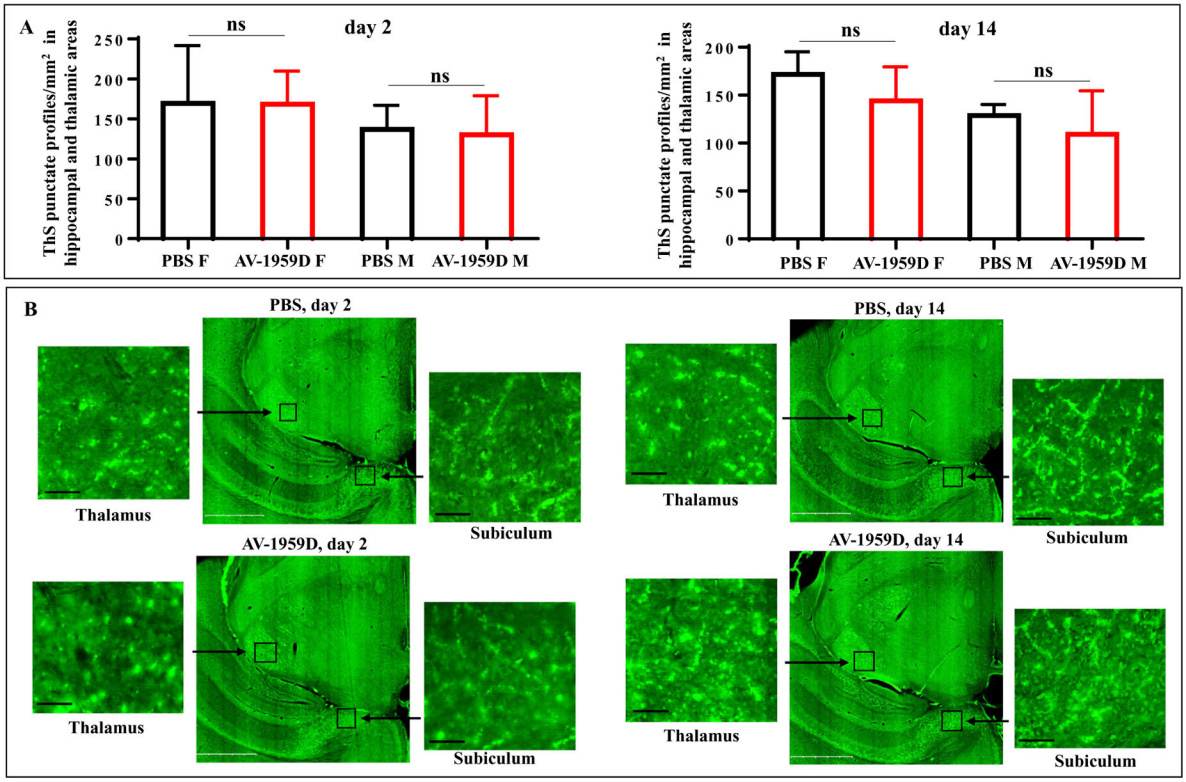

Fig. 8.

No increase in vascular deposition of Aβ was observed in AV-1959D/EP vaccinated Tg-SwDI mice of $H2^b$ haplotype compared with control animals 2 and 14 days after the last immunization. (A) 10–11 mo old Tg-SwDI mice were vaccinated with 50 μg/mouse of AV-1959D at days 0, 14, 44, 74 and mice were terminated at days 2 and 14 after the last immunization (n = 8/gender/time point for experimental and 7/gender/time point for control groups). Brain sections were stained with ThS followed by the quantitative data analyses of the punctate ThS-stained blood vessel profiles in the CAA-prone hippocampal and thalamic regions of mouse brains. Bars represent average ± SEM. (B) Photomicrographs depict representative half brain slices showing hippocampal and thalamic areas on the same plane for every analyzed group. Boxed areas depict high-power views of CAA profiles in subiculum and thalamus. Scale bars: low magnification = 1 mm, enlarged images = 50 μm.

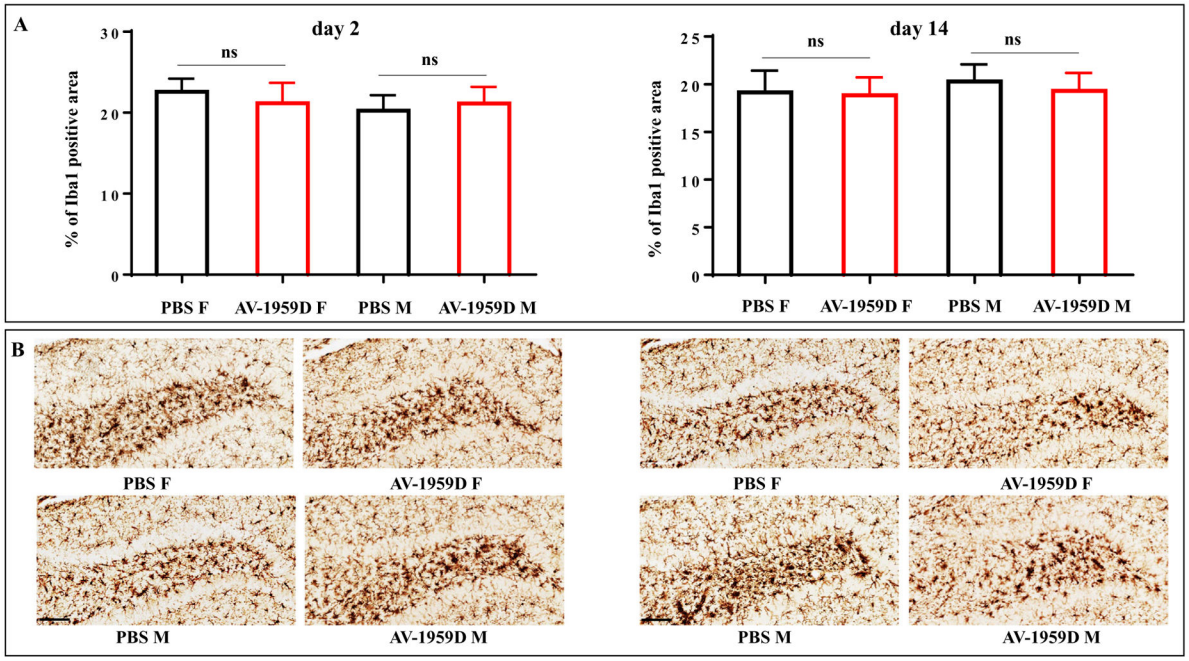

Fig. 9.

No increase in microglia activation was observed in AV-1959D/EP vaccinated Tg-SwDI mice compared with control animals 2 and 14 days after the last immunization. (A) Bars represent the average percent of Iba-1 positive area ± SEM. (B) Photomicrographs of representative images show reactive microglia in the hilar region of dentate gyrus vs. hyper-ramified microglial profiles in the adjacent layers in the brains of immunized (n = 8/gender/time point) and control (n = 7/gender/time point) female (F) and male (M) mice. Scale bars = 100 μm.

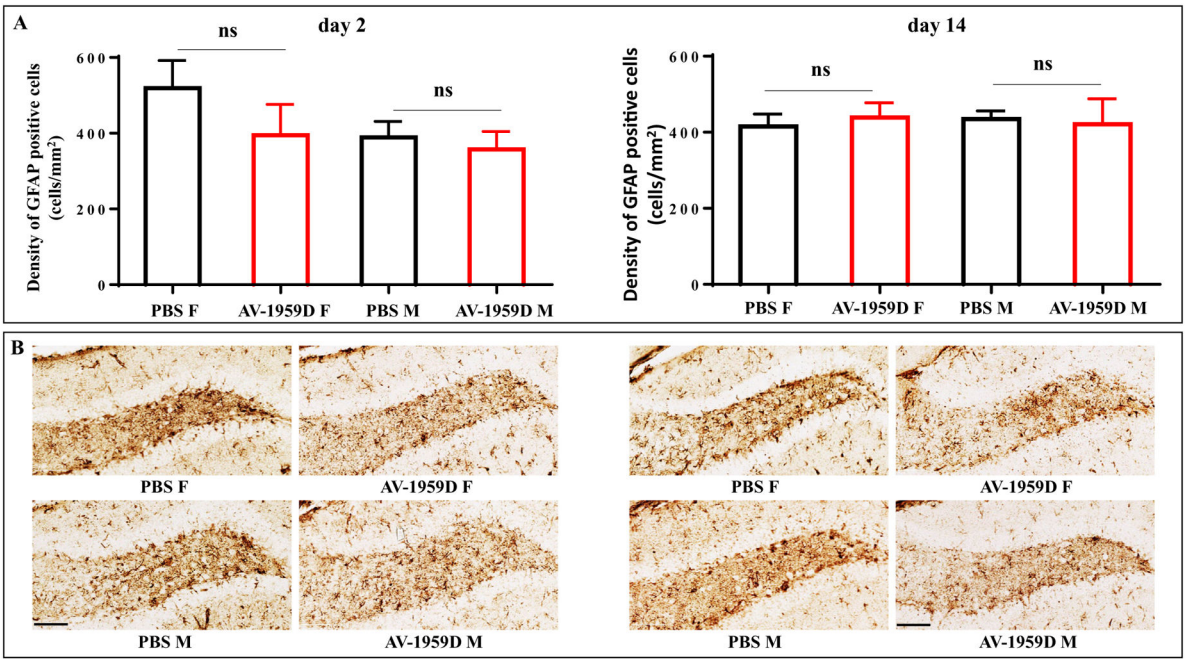

Fig. 10.

No increase in astrocyte activation was observed in AV-1959D/EP vaccinated mice compared to control animals 2 and 14 days after the last immunization. (A) Bars represent the average density of GFAP positive cells ± SEM. (B) Photomicrographs of diffuse reactive astrogliosis in the hilar region of dentate gyrus with pronounced upregulation of GFAP expression and overlap of the astrocyte processes vs. mild to moderate reactive astrogliosis in adjacent layers in the brains of immunized (n = 8/gender/time point) and control (n = 7/gender/timepoint) female (F) and male (M) mice. Scale bars = 100 μm.

Lymphocyte infiltration	day 2 (average ±SEM)			day 14 (average ±SEM)		
	PBS	AV-1959D	*P value*	PBS	AV-1959D	*P value*
CD3⁺ T cells	2.0±0.46	1.0±0.25	*0.0838*	2.0±0.39	0.88±0.17	*0.0093*
B cells (B220)	1.6±0.30	1.077±0.33	*0.2547*	1.35±0.32	1.23±0.16	*0.7254*

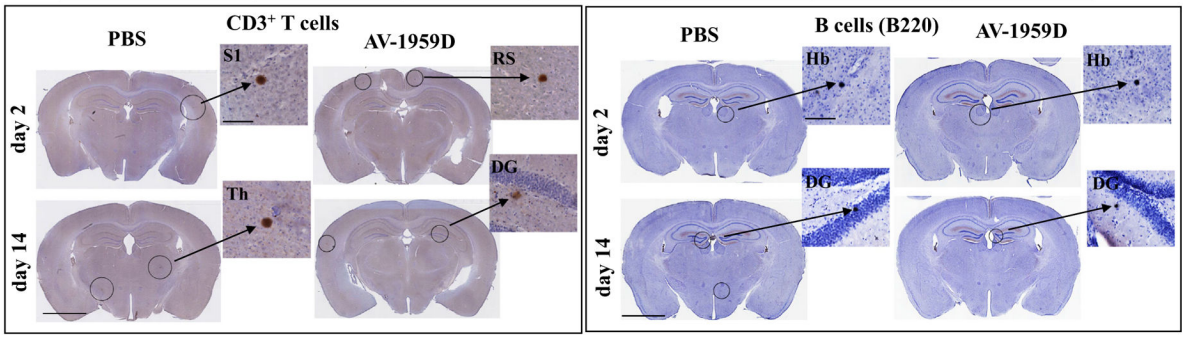

Fig. 11.

No increased infiltration of T and B cells was observed in AV-1959D/EP vaccinated mice compared with control animals 2 and 14 days after the last immunization. Table represents average number ± SEM of the infiltrating lymphocytes per brain section. Photomicrographs of the brain sections from immunized (n = 8/gender/time point) and control (n = 7/gender/timepoint) mice stained with anti-CD3 and anti-B220. High-power views are taken from the circled areas: S1 (primary somatosensory cortex), RS (retrosplenial cortex), Th (thalamic nucleus), DG (dentate gyrus), Hb (habenular nucleus). Scale bars: low magnification = 2.5 mm, enlarged images =100 μm.

Neurodegeneration	day 2 (Average ±SEM)			day 14 (Average ±SEM)		
	PBS	AV-1959D	*P value*	PBS	AV-1959D	*P value*
Necrotic/apoptotic cells (TUNEL)	0.8±0.2	0.538±0.18	*0.3492*	0.57±0.22	0.7±0.16	*0.6298*
Caspase-3 positive area mm^2	58.67±12.8	60.15±14.44	*0.9389*	56.36±11.35	66.88±12.69	*0.5494*

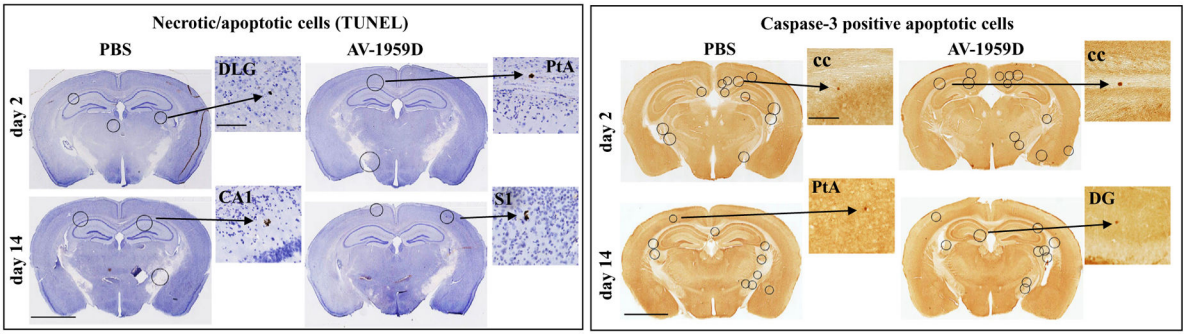

Fig. 12.

No increase in the number of necrotic/apoptotic cells was observed in AV-1959D/EP vaccinated mice compared with control animals 2 and 14 days after the last immunization. The Table summarizes the average number ± SEM of TUNEL-positive cells and anti-caspase-3-positive area per brain section. Photomicrographs of brain sections from immunized (n = 8/gender/time point) and control (n = 7/gender/timepoint) mice analyzed via TUNEL for nuclear fragmentation and formation of apoptotic bodies, and anti-caspase-3 immunostaining for apoptosis. High-power images taken from circled areas: DLG (dorsal lateral geniculate nucleus of thalamus), PtA (parietal association cortex), CA1 (field CA1 of hippocampus), S1 (primary somatosensory cortex), cc (corpus callosum), DG (dentate gyrus). Scale bars: low magnification =2.5 mm, enlarged images =100 μm.

Table 1

Biodistribution/persistence study.

Group	Agents Tested	Delivery	Immunization schedule (Day 0)	Necropsy (Day 2)	Necropsy (Day 60)
1	PBS	ID/EP	1	5 M/5F	5 M/5F
2	AV-1959D in PBS	ID/EP	1	8 M/8F	8 M/8F

Table 2

Repeat dose acute and long-term toxicology study.

Group	Agents tested	Dose Level (μg/ mouse)	Delivery	Immunization schedule (Days)	Sacrificial end-points		
					Day 76	Day 102	Day 158
					2 days after last immunization	1 month after last immunization	3 months after last immunization
1	PBS		ID / EP	1, 14, 44, 74	10 M / 10F	10 M / 10F	10 M / 10F
2	AV-1959D	5	ID / EP	1, 14, 44, 74	10 M / 10F	10 M / 10F	10 M / 10F
3	AV-1959D	25	ID / EP	1, 14, 44, 74	10 M / 10F	10 M / 10F	10 M / 10F
4	AV-1959D	50	ID / EP	1, 14, 44, 74	10 M / 10F	10 M / 10F	10 M / 10F